1. Theoretical Solid State Physics

Theoretical research in solid state physics is generally planned to complement the experimental programs of the Division. The emphasis of the theoretical work is therefore determined in large part by the experimental programs currently under way. An example of the close interplay between the theoretical and experimental research occurs in the area of surface physics. As the importance of the surface program in the Division has grown in the last few years, virtually every member of the Theoretical Section has tackled one or more surface-related problems. Of course, theoretical research in other areas traditionally of interest to the Division has also continued. The overall program of theoretical research can be loosely grouped into the four categories of surface studies, particle-solid interactions, electronic and magnetic properties, and lattice dynamics.

Because of its relevance to materials problems of advanced energy systems, research in the area of surface physics continues to grow in the Solid State Division. During the period covered by this annual report, studies of the reflection of light atoms from solid surfaces have continued. This work is particularly important for the plasma-stability problem in fusion reactor design because hydrogen recycling between the walls and the plasma can lead to important consequences in the particle and energy balances of the system. Work has also continued on the interpretation of surface-related data generated by low energy electron diffraction (LEED) and Auger experiments. Recently, a model has been developed that provides the first consistent interpretation of angular dependent Auger spectroscopy (ADAS) data. Further refinement of the model will be pursued in order to determine the applicability of the ADAS technique to surface studies. A new study commenced during the past year seeks to determine if radiative electron capture (REC) by channeled ions can be used to extract information about the surface properties of solids.

Theoretical studies of particle-solid interactions are concerned with the interpretation of phenomena that are manifest when energetic particles are scattered by the atoms of a solid. Some of the problems studied, such as radiation damage in metals, are of direct relevance to technical problems in the development of both fission and fusion reactors. Others, such as channeling, are primarily of interest either to fundamental studies of solids or to detailed studies of the atomic collisions themselves. During the past year, work on the use of computer simulation to interpret channeling experiments has continued, with particular emphasis on extracting information about atomic relaxation in solids and interplanar spacing of atoms at surfaces. This work is a good example of how a technique originally applied to the determination of bulk properties can be modified to yield information about surface properties as well. Another investigation of particular significance is concerned with the determination of displacement cascade lifetimes in monatomic solids. The cascade lifetime is important in treating such problems as thermal spikes and space-time coincidences of displacement cascades. A method has been developed that enables one to calculate the displacement cascade lifetime more precisely than in the past.

BLANK PAGE

In the area of electronic and magnetic properties, two studies stand out as being of particular interest. One of these is the continued development of large cluster calculations to simulate bulk electronic properties of alloys and of crystals containing isolated point defects. In cluster calculations, a real solid with an essentially infinite number of atoms is replaced by a cluster containing a finite number of atoms. The objective of this study is to develop computational techniques that allow the inclusion of large numbers of atoms in the cluster in order to simulate the properties of the real solid accurately. The other study involves calculating the magnetic exchange interaction in the heavy rare earth metals. It has now been demonstrated that the measured spin-wave dispersion curves in these metals can be explained without invoking the anomalously large two-ion anisotropy previously proposed for these systems. The existence of such a large anisotropy has always been difficult to understand. Work has continued on the extension of the augmented space formalism to disordered systems with short-range order.

Research on lattice dynamics covers a wide variety of calculations on the vibrational properties of perfect crystals, random alloys, crystals containing point imperfections, and crystal surfaces. Recently a major thrust of the lattice dynamical work has been in the direction of large cluster calculations described in the preceding paragraph in connection with electronic properties. Another important focus of the research in this area is on the interaction between internal vibrational modes of molecular-like impurities and the phonons of the host crystal. Under favorable conditions, this interaction can lead to observations by inelastic neutron scattering of impurity-induced effects at very small impurity concentrations. The much-discussed recent work in the Division on self-interstitials in fcc metals falls into this class of problems. Another example is the CN^- impurity in KCl, which was the first molecular impurity studied by neutron scattering. This system has the advantage over self-interstitials in metals as a model system, because the CN^- molecule can be substituted for Cl^- over a wide range of concentrations. Calculations have also continued on the "first-principles" evaluation of phonon dispersion curves in high T_c superconductors. This very intricate computational problem now appears to be nearly solved.

SURFACE STUDIES

TEMPERATURE EFFECTS IN LEED

H. L. Davis

Low energy electron diffraction (LEED) is an established technique for the investigation of surfaces.[1] Information concerning the symmetry of a surface is obtained directly from LEED intensity patterns. More detailed information about surface crystallography can be obtained when LEED beam intensities are measured as a function of the incident electron energy and compared with calculated results.[2] These calculations must incorporate the multiple scattering of the electrons by the atoms in the surface region. We have found an interesting illustration of the importance of multiple-scattering effects in recent work analyzing temperature effects in LEED data for a Cu (100) surface.

Information concerning the vibrations of surface atoms is potentially available from LEED experiments when reflected beam intensity data are collected as a function of temperature. For example, (00) beam data collected by Reid[3] from a Cu (100) surface (Fig. 1.1) reveals that an increase in temperature produces a dramatic reversal in the relative intensities of the two major peaks found in the data: at 340 K the peak at 41 eV is more intense than the peak at 35 eV, while at 810 K the reverse is true. If an analysis like that usually employed for temperature-dependent x-ray or neutron scattering data from bulk samples were used to interpret the data of Fig. 1.1, a different Debye temperature would be obtained for each peak. The temperature dependence of the peak at 35 eV corresponds to a surface Debye temperature of approximately 300 K, while that of the 41-eV peak corresponds to a Debye temperature of approximately 200 K. For comparison, the Debye temperature for bulk copper is about 340 K. As we have shown by using techniques and computer codes reported previously, this apparent discrepancy in Debye temperatures is just a

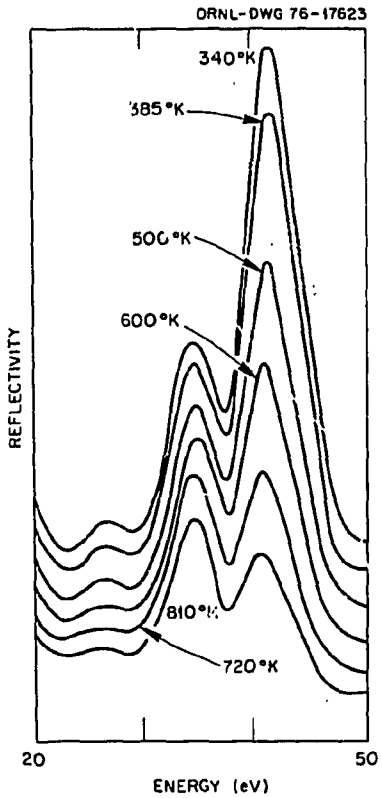

Fig. 1.1. Data for the (00) beam from the Cu (100) surface obtained by Reid (ref. 3). The incident electron beam was aligned so that $\theta = 11°$ and $\phi = 3°$.

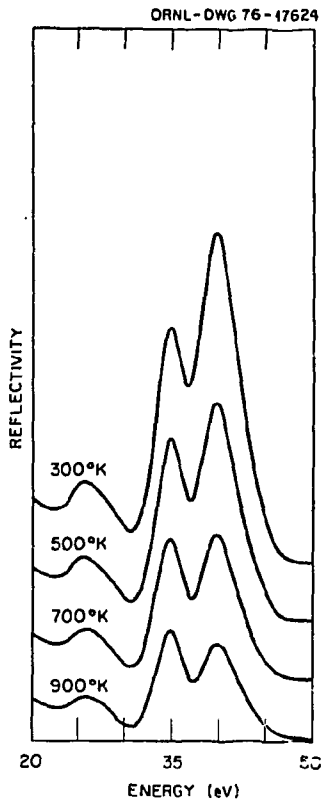

Fig. 1.2. The results of calculations described in the text for the (00) beam from the Cu (100) surface. The calculations employed $\theta = 11°$ and $\phi = 3°$.

consequence of the multiple-scattering process suffered by the incident electrons.[4] In contrast, a single scattering treatment is usually sufficient to interpret x-ray or neutron data.

Using a single surface Debye temperature of 250 K, we based our LEED calculations on the theory of multiple electron scattering in a vibrating lattice.[5-7] Results are given in Fig. 1.2. The elastic scattering processes were accounted for by employing phase shifts obtained from the copper potential of Snow and Waber;[8] the inelastic scattering was mimicked by using an amplitude attenuation mean free path of 13 Å. A comparison of Figs. 1.1 and 1.2 shows that quantitative agreement with Reid's data can be obtained using a single surface Debye temperature, provided that multiple-scattering processes are correctly included in the theory. The use of a surface Debye temperature of 250 K in the calculations rather than the bulk value of 340 K is physically reasonable, because we expect surface atoms to vibrate with larger amplitudes than do atoms in the bulk.

1. See, for example, J. B. Pendry, *Low-Energy Electron Diffraction*, Academic Press, New York, 1974.
2. An illustration of surface crystallography may be seen in J. R. Noonan, H. L. Davis, and L. H. Jenkins, "LEED Analysis of the Cu (110) Surface," this report.
3. R. J. Reid, *Phys. Status Solidi A* **4**, K211 (1971).
4. H. L. Davis, *Solid State Div. Annu. Prog. Rep. Dec. 31, 1975*, ORNL-5135, p. 5.
5. C. B. Duke and G. E. Laramore, *Phys. Rev. B* **2**, 4765 (1970).
6. G. E. Laramore and C. B. Duke, *Phys. Rev. B* **2**, 4783 (1970).
7. B. W. Holland, *Surf. Sci.* **28**, 258 (1971).
8. E. C. Snow and J. T. Waber, *Phys. Rev.* **157**, 570 (1967).

LATTICE VIBRATIONS AT SURFACES

Mark Mostoller Theodore Kaplan

Not only are the vibrational properties of atoms in the surface region of a solid of intrinsic interest, but

they also enter the detailed interpretation of data from such surface probes as low energy electron diffraction (LEED) and ion backscattering. It is well known, for example, that the t-matrices which describe the scattering of electrons from atoms in the surface region should incorporate Debye-Waller factors which arise from the surface vibrations.[1] In general, these surface vibrations may be expected to exhibit considerable anisotropy.

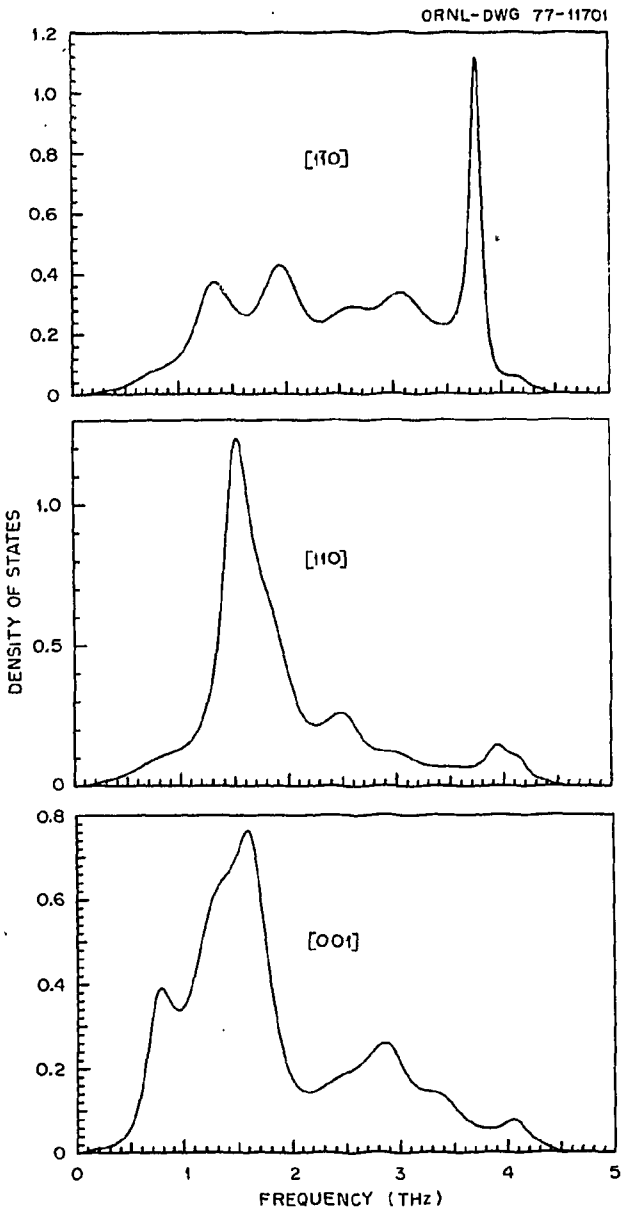

Fig. 1.3. Densities of states for vibrations of an atom in an unrelaxed Au (110) surface along the [1$\bar{1}$0], [110], and [001] directions.

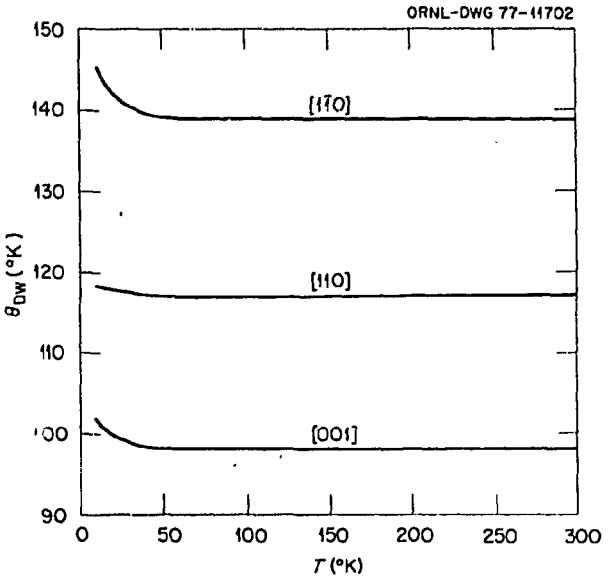

Fig. 1.4. Effective Debye-Waller temperatures $\theta_{DW}(T)$ for the three surface vibrational densities of states shown in Fig. 1.3.

Computer programs have been developed to calculate the densities of states and vibrational correlation functions for atoms in the surface region, using the recursion method described in another contribution to this report.[2] Recursion calculations can be performed within clusters of thousands of atoms, with first-nearest-neighbor or first- and second-neighbor interactions included. Figure 1.3 shows the results of one such calculation of the densities of states for vibrations of an atom in a Au (110) surface along the [1$\bar{1}$0], [110], and [001] directions: the first and last of these directions are in the surface; the middle is normal to the surface. These results were obtained with first-neighbor force constants fitted to the bulk neutron scattering measurements of Lynn, Smith, and Nicklow[3] with recursion applied after level 11 in a 12-level cluster of 4192 atoms. Figure 1.4 shows the Debye-Waller temperatures derived from the mean square amplitudes of vibration along the three directions. For comparison, the bulk Debye-Waller temperatures $\theta_{DW}(T)$ are about 170 K and 165 K for low and high T respectively. Figures 1.3 and 1.4 illustrate the anisotropy of surface vibrations.

At present, the computer programs for surface vibrations do not include surface relaxation or

anharmonic effects, both of which are expected to be important. Work will be undertaken to include these effects in the near future.

---

1. J. B. Pendry, *Low-Energy Electron Diffraction*, Academic Press, New York, 1974.
2. Mark Mostoller and Theodore Kaplan, "Cluster Calculations: Simulation of Bulk Properties," this report.
3. J. W. Lynn, H. G. Smith, and R. M. Nicklow, *Phys. Rev. B* **8**, 3493 (1973).

ANALYSIS OF ANGULAR-DEPENDENT AUGER SPECTROSCOPY BASED ON A QUASIATOMIC MODEL

H. L. Davis

Theoretical studies concerning the possible utilization of angular-dependent Auger spectroscopy (ADAS) as a tool for surface analysis have continued. By ADAS we denote measurements of the angular variations in the current of Auger electrons emitted from a surface, with the detector tuned to detect only those electrons which correspond to a specified Auger transition. Several recent experimental[1-4] and theoretical[2,5-7] ADAS studies have been made. These investigations, and this work, have been motivated by the hope that ADAS might prove to be a useful tool for surface crystallography and/or the determination of surface electronic structure.

ADAS might be useful for crystallography because the Auger electrons (after emission) are scattered by the atoms in the surface; this scattering may be responsible for some of the large angular variations observed in ADAS. It could also be useful for electronic structure determination if significant angular variations are due to inherently anisotropic Auger emission. That is, the electronic structure of the surface region could influence transition probabilities and be reflected in the anisotropic emission.

For ADAS to evolve further as a tool for surface studies, it would be helpful to demonstrate that present theoretical treatments are capable of reproducing observed ADAS signals. To provide a partial demonstration of this, we have developed a model that gives results in good agreement with some of the $M_{2,3}VV$ data obtained from a Cu (100) surface.

In any theoretical ADAS calculations, two dominant aspects of the relevant physics must be considered and modeled. First, the wavefield emitted during the Auger transition process must be either calculated or otherwise specified. Second, it is essential to consider how this emitted wave escapes the sample, that is, how the emitted Auger electron scatters from the other atoms in the surface region before it reaches a detector. The necessary formalism has been developed[5] to treat the scattering aspects, provided that each Auger emission event is represented by a single (or a linear combination of) partial wave(s) of the form

$$I_{lm}(\mathbf{r};\mathbf{r}_n) = \kappa^{1/2} B_{lm} h^{(1)}(\kappa|\mathbf{r}-\mathbf{r}_n|)\, Y_{lm}(\mathbf{r}-\mathbf{r}_n) ,$$

where $I_{lm}(\mathbf{r};\mathbf{r}_n)$ is the amplitude at r of an (l,m) partial wave emitted at the atomic site $\mathbf{r}_n$. The wave number $\kappa = (E - V_0)^{1/2}$ is complex: E is the energy of the emitted Auger electron outside the sample, and V_0 is a complex background potential for the electron inside the sample. The probability per unit time of an emission with (l,m) character is given by $|B_{lm}|^2$.

Some calculations[2,6,7] have been reported in which every Auger emission was taken to be a single partial wave of fixed (l,m) character. Although none of this work has successfully reproduced an experimental ADAS signal, it has made it possible to reach some conclusions about, say, the $M_{2,3}VV$ Cu ADAS. These conclusions are (1) it is essential that a full multiple-scattering treatment of the emitted Auger wavefield be employed in ADAS calculations; (2) the calculations do predict angular variations of the same magnitude as those observed experimentally; (3) inherent anisotropy in the Auger emission must be responsible for some of the angular variations observed; and (4) no single (l,m) partial wave emission will fit the experimental ADAS results.

In the present work, a quasiatomic model has been invoked. Basic to the model is the assumption that each individual emission event corresponds to a single (l,m) wave but that (l,m) may vary from emission to emission. The total ADAS signal is then the weighted sum of *intensities* from all possible (l,m) emissions. Of course, a priori determination of (l,m) weights would require that Auger transition matrix elements be calculated which, in turn, would require that the features of copper's electronic structure in the surface region be incorporated into the model. Rather than perform such calculations, we decided first to try to estimate the (l,m) emission weights by fitting calculated ADAS intensity profiles to the experimental data.

Figure 1.5 compares our calculated results to some of the $M_{2,3}VV$ Cu (100) ADAS data of Noonan, Zehner, and Jenkins.[2] In Fig. 1.5, the angles θ and ϕ describe the angular position of the detector, with θ being relative to the surface normal and ϕ relative to the [010] direction. To obtain this fit, we first

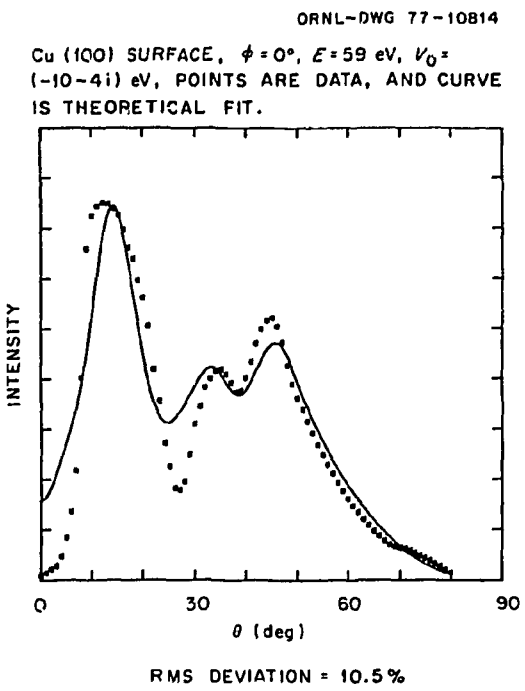

Fig. 1.5. Fit (solid curve) to the $M_{2,3}VV$ Cu (100) ADAS data (points) for $\phi = 0°$ when all four distinct $l = 3$ sources are used. Weights determined were 0.080, 0.246, 0.124, and 0.550, respectively, for $m = 0, \pm 1, \pm 2$, and ± 3.

calculated individual intensity profiles for all (l,m) values up to $l = 5$. For (l,m) fixed, an individual intensity profile is the weighted sum of intensities for this emission originating in each of the atomic layers in the surface region. The intensity for each layer was calculated by employing the multiple-scattering formalism of Pendry,[5] with an extra factor of $\cos\theta$ included in the final result. Since the experimental results were obtained by stimulating the emission by bombardment with 350-eV electrons, the layer intensities were weighted by probability factors for layer emission to occur. The final (l,m) intensity profiles were then broadened to simulate the 4.3° angular resolution of the detector. We employed bulk copper lattice spacings, $E = 59$ eV, $V_0 = (-10 - 4i)$ eV, 3 to 5 passes of renormalized forward-scattering perturbation theory, 25 layer reciprocal lattice vectors, and 7 phase shifts calculated from the Chodorow potential.[8]

For $l \leq 5$ there exist 36 (l,m) combinations, but the intensity profiles for $(l,\pm m)$ are identical by symmetry, leaving 21 distinct (l,m) contributions to consider. In the least squares procedures used to fit various combinations of these 21 profiles to the ADAS data, we considered all combinations, n at a time, for $n = 2$–6. It was first determined whether a given combination produced a valid fit, with a valid fit being one in which all emission weights were found to be positive. The root-mean-square (rms) deviations of the valid fits were calculated, and those fits with the smaller rms deviations were plotted for visual inspection. Figure 1.5 gives one of the best fits obtained using combinations of the calculated (l,m) profiles four at a time. Of the possible 5985 combinations, approximately 1400 resulted in valid fits. However, almost all the valid fits had rms deviations greater than 15% relative to the maximum peak intensity of the data. The rms deviation of the fit of Fig. 1.5 is 10.5%.

The procedures we employed contain some inadequacies; however, Fig. 1.5 demonstrates that the model gives reasonable agreement with the data. This good fit probably is more than fortuitous and indicates that the model reflects considerable physical reality. Moreover, the good fit achieved involves only $(3,m)$ sources, which is consistent with the work of Feibelman and McGuire,[9] who considered only the Auger line shape and not the ADAS process. Thus a reinforcing self-consistency has emerged from the model.

Both the individual layer contributions and the contributions of the separate $(3,m)$ sources to the total calculated intensity shown in Fig. 1.5 merit attention. Figure 1.6 illustrates the contributions of

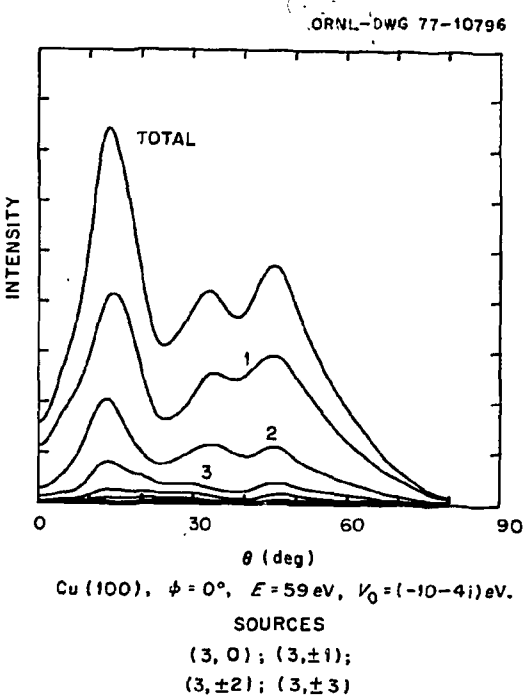

Fig. 1.6. Contributions of the individual surface layers to the total calculated intensity of Fig. 1.5.

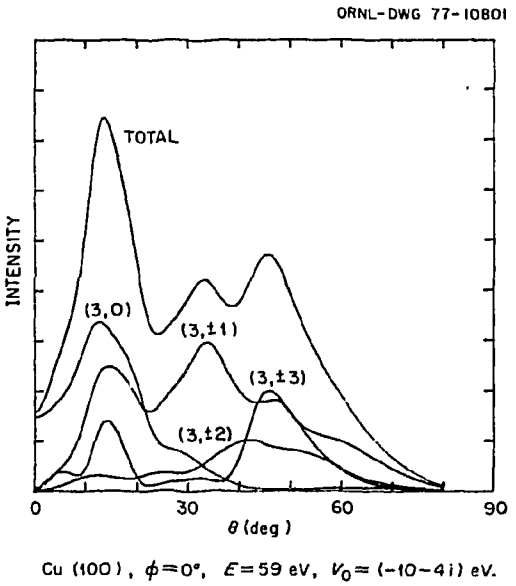

Fig. 1.7. Contributions of the separate $l=3$ sources to the total calculated intensity of Fig. 1.5. The curves are labeled by the respective values of m.

the layers and indicates that only the first few contribute significantly to the total. Figure 1.6 also shows that almost all of the peak structure present is caused by emission occurring in the first two layers of the surface. Figure 1.7 shows the contributions of the separate $(3,m)$ sources to the total, and it is clearly seen that more than one (l,m) emission is required to explain the structure in the data. Almost all of the peak structure is due to only three distinct sources: $(3,\pm3)$, $(3,\pm1)$, and $(3,0)$.

When fits were attempted using (l,m) profiles in combinations of five or six at a time, the results obtained were only slightly better than those shown in Fig. 1.5. It should be noted that, regardless of the number of (l,m) combinations used in the fitting, valid fits with small rms deviations always had a calculated intensity at $\theta = 0°$ of the magnitude shown in Fig. 1.5. We do not know the reason for this specific discrepancy but believe it merits further investigation. To test further the validity of the present model, we have undertaken treatments of more Cu (100) data[2] and of Cu (110) data.[3]

1. L. McDonnell, D. P. Woodruff, and B. W. Holland, *Surf. Sci.* 51, 249 (1975).
2. J. R. Noonan, D. M. Zehner, and L. H. Jenkins, *J. Vac. Sci. Technol.* 13, 183 (1976).
3. D. M. Zehner, J. R. Noonan, and L. H. Jenkins, *Solid State Commun.* 18, 483 (1976).
4. G. Allié, E. Blanc, and D. Dufayard, *Surf. Sci.* 57, 293 (1976).
5. J. B. Pendry, *J. Phys. C* 8, 2413 (1975).
6. H. L. Davis and T. Kaplan, *Solid State Commun.* 19, 595 (1976).
7. D. Aberdam et al. *Surf. Sci.* 57, 306 (1976).
8. M. I. Chodorow, *Phys. Rev.* 55, 675 (1939).
9. P. J. Feibelman and E. J. McGuire, *Phys. Rev. B* (to be published).

THEORY OF RADIATIVE ELECTRON CAPTURE BY CHANNELED IONS

M.V.K. Ülehla[1] H. L. Davis

Recently Koyama and Ohtsuki[2] have considered the process in which a crystal is bombarded by an ion that in turn captures an electron from the crystal. In particular, these authors considered in detail one specific mechanism for this reaction to proceed—radiative electron capture (REC). In REC, the ion interacts with the crystal and captures one of the valence electrons; the excess electronic energy is given off as an x ray. Koyama and Ohtsuki proposed a model for REC in which a metal's surface electronic structure was accounted for in a simple manner. Their calculated results for the REC cross section appeared to reproduce both the shape and magnitude of the experimental cross section obtained by Appleton et al.,[3] who bombarded a silver single crystal with O^{8+} ions with energies in the 15- to 40-MeV range (see Fig. 1 of ref. 2). The experimental cross section increases with increasing energy, which is in sharp contrast to the Bethe-Salpeter formalism[4] of REC, which predicts a decrease with increasing energy. Since the model employed by Koyama and Ohtsuki contains a critical surface feature and appeared to produce results in good agreement with experimental data, it could be inferred that REC might prove to be a useful tool for investigating the electronic structure of surfaces. However, while attempting to reproduce their results, we have established that the agreement with experiment that they obtained is erroneous and accidental. Their results do not in fact follow from the model they employed, because an error was made in their evaluation of the integrals occurring in the expression for the REC cross section.

In the model of Koyama and Ohtsuki, the crystal's electrons are confined to a semi-infinite square-step potential with the step at the surface of the crystal, $z = 0$. The step has depth U_0, which is the sum of the Fermi energy and the work function of the metal. The

cross section, σ_{REC}, for a specific electron capture event is found to depend on U_0, on the energy of the bombarding ion, and on the electron's wave vector components $k_\parallel$ and $k_\perp$ parallel and perpendicular to the surface. Using this model, we have calculated σ_{REC} in the dipole approximation for a case that could correspond to O^{8+} ions bombarding a silver crystal. The results are compared in Fig. 1.8 with the experimental data of Appleton et al.[3] Our calculated curve in Fig. 1.8 was obtained using $U_0 = 10.3$ eV, $k_\parallel = k_\perp = k_F/2$, and an electron density (i.e., k_F) corresponding to one-half electron per silver site. Also plotted in Fig. 1.8 is the cross section one obtains if the Bethe-Salpeter formalism[4] is applied to ions having $Z = 8$.

The theoretical model used here and in ref. 2 for REC in metals does provide some improvement over the standard Bethe-Salpeter formalism; generally the magnitude of the cross section is larger and agrees more closely with that obtained experimentally. However, we have found no physically reasonable choice of the model parameters ($U_0, k_\parallel, k_\perp$) that will yield a rise in cross section with ion energy such as that found experimentally.

Because this simple model does provide an improvement in cross-section magnitude, it is probably worthwhile to consider other REC models in which the metal's surface features are taken into account in various ways. Work along these lines is now in progress. At the same time, we expect to consider REC models that treat electrons in the bulk of the crystal more realistically.

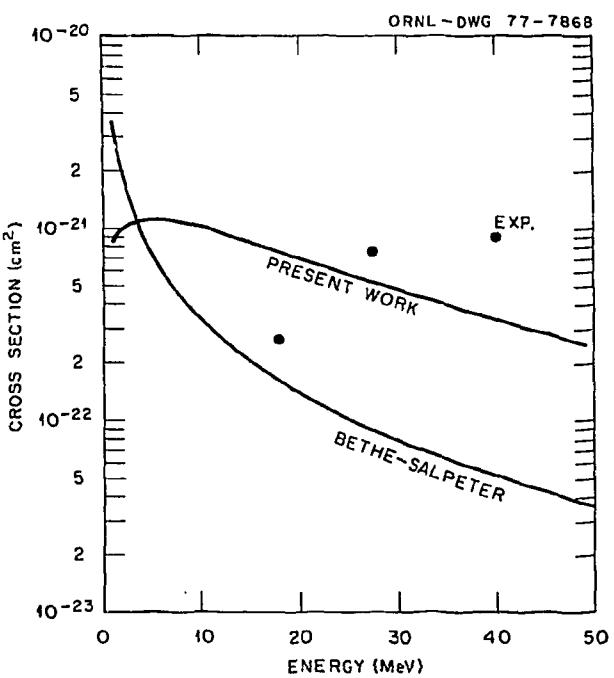

Fig. 1.8. Present calculation for REC cross section is compared with experimental data and Bethe-Salpeter result.

1. Eugene P. Wigner Fellow.
2. K. Koyama and Y. H. Ohtsuki, *Phys. Rev. B* 15, 61 (1977).
3. B. R. Appleton et al., p. 499 in *Atomic Collisions in Solids*, ed. by S. Datz, B. R. Appleton, and C. D. Moak, Plenum Press, New York, 1975.
4. H. Bethe and E. E. Salpeter, p. 320 in *Quantum Mechanics of One- and Two- Electron Atoms*, Academic Press, New York, 1957.

COMPUTER STUDIES OF THE SCATTERING OF LOW-ENERGY HYDROGEN IONS FROM POLYCRYSTALLINE SOLID SURFACES

O. S. Oen M. T. Robinson

Hydrogen recycling between the walls and the plasma in a controlled fusion reactor can lead to important consequences in the particle and energy balances of the system.[1] The hydrogen ions, through charge exchange, will escape a magnetically confined plasma and bombard the first wall of the containment vessel. A fraction of the hydrogen will be reflected (backscattered) from the walls back into the plasma with reduced energy while the remainder will slow down and come to rest within the walls. For reactor design, it is necessary to know the amount and the energy distribution of the reflected hydrogen. Although the backscattering of hydrogen ions with energies above 100 keV has been studied extensively for many years, only a limited amount of experimental and theoretical work has been done for incident energies of a few keV or less, which is the region of most interest to current fusion research. Experimentally, the problem is greatly complicated by the difficulty in detecting the low-energy reflected neutral atoms.

A comprehensive calculational program[2] was initiated some time ago to study the interaction of low-energy light ions with solid surfaces using the binary collision cascade program MARLOWE. Results have been reported previously for amorphous solid targets.[3]

Those studies have been extended to polycrystalline targets.[4] This extension is necessary because most experimental targets possess sufficient crystalline texture to affect the motion of the ions

through channeling. We have calculated the reflection of 50-eV to 10-keV hydrogen atoms from polycrystalline copper, niobium, and gold. It was found that the effects of polycrystallinity are modest, reducing the amorphous reflection coefficients by about 25%. No specific differences were found between the bcc (niobium) and the fcc (copper and gold) polycrystalline calculations. Our results for the fraction of particles reflected agree quite well with experimental data for copper and gold[5] but are about a factor of 2 larger for niobium. For the fraction of energy reflected, the results of our calculations are somewhat higher than observed, especially at the higher energies. Again, poorest agreement was found for niobium targets, where the calculated values are about a factor of 2 greater than observed. There are at least three possible reasons for this: the electronic stopping assumed in the calculations may be too low; oxide layers, which were not included in the calculation, may be present in the experimental targets; or there may be more crystalline texture in the targets than assumed in the calculation.

The experimental work to date has been carried out at a relatively high energy (>5 keV) with respect to current fusion needs. Until experimental information at low energy becomes available, the present calculations can serve as a guide for the design of controlled fusion reactors.

1. J. T. Hogan and J. F. Clarke, *J. Nucl. Mater.* 53, 1 (1974).
2. M. T. Robinson and O. S. Oen, *Solid State Div. Annu. Prog. Rep. Dec. 31, 1974*, ORNL-5028, p. 16.
3. O. S. Oen and M. T. Robinson, *Nucl. Instrum. Methods* 132, 647 (1976).
4. O. S. Oen and M. T. Robinson, *J. Nucl. Mater.* 63, 210 (1976).
5. See ref. 3 for references to experimental data.

ANALYTICAL SOLUTIONS TO THE TWO-PARTICLE BLOCKING MODEL

O. S. Oen

A renewed interest in the two-particle blocking (shadowing) model[1] has been sparked by recent ion-scattering experiments from crystalline surfaces in which only one or at most a few atoms contribute to the blocking pattern. For many surface cases, for instance, the two-particle model gives close agreement with Monte Carlo simulations[2] that include all the row atoms. The model, therefore, has been reinvestigated, and an analytical solution has been found. From ref. 1, the expression for the emission pattern at angle θ is

$$F(\theta) = \int_0^\infty \frac{2s\,ds}{\rho^2} I_0\left\{\frac{2l\theta[s + l\phi(s)]}{\rho^2}\right\} \times \exp\left\{-\frac{[s + l\phi(s)]^2 + (l\theta)^2}{\rho^2}\right\}, \quad (1)$$

where l is the distance between emitting and scattering centers, ρ^2 is the mean square thermal displacement amplitude, and $I_0(x)$ is the modified Bessel function of the first kind. Here, $\phi(s)$ is the scattering function for impact parameter s. In our previous work, Eq. (1) was evaluated numerically. However, for a Coulomb potential an exact analytical solution has been found to be

$$F(\theta) = \frac{\beta^2}{2} \exp\left[-\left(\alpha^2 + \frac{\beta^2}{2}\right)\right] \sum_{k=0}^{\infty}\left[\left(\frac{\alpha\beta}{2}\right)^{2k} \frac{1}{(k!)^2} \sum_{r=0}^{2k} \frac{(2k)!}{(2k-r)!r!} K_{r+1-k}\left(\frac{\beta^2}{2}\right)\right], \quad (2)$$

where $K_r(s)$ is the modified Bessel function of the third kind, $\alpha = l\theta/\rho$, and $\beta = l\theta_c/\rho$. The quantity $\theta_c = 2\sqrt{Z_1 Z_2 e^2/lE}$, with E the projectile kinetic energy, is the critical blocking angle for the static case. Equation (2) gives the very important result that $F(\theta)$ is a function of *only two parameters*, α and β. Thus a complete solution can be displayed by a single contour plot. For scattering from a screened Coulomb potential, such as the Molière potential, an analytical solution to Eq. (1) appears difficult. However, the Coulomb results suggest that a similar parameterization in which the Coulomb critical angle is replaced by the Molière critical angle may work. This was done and a nearly universal set of curves over a wide range of parameter values was found.

1. O. S. Oen, *Phys. Lett.* 19, 358 (1965).
2. J. H. Barrett, "Use of Computer Simulation to Interpret Channeling Experiments," p. 571 in *Proceedings, Fourth Conference on Scientific and Industrial Applications of Small Accelerators*, ed. J. L. Duggan and I. L. Morgan, IEEE 76CH1175-9 NTS, Piscataway, N.J., 1977; J. H. Barrett, same title, this report.

PARTICLE-SOLID INTERACTIONS

USE OF COMPUTER SIMULATION TO INTERPRET CHANNELING EXPERIMENTS[1]

John H. Barrett

Computer simulations[2] have been used to extract information from channeling experiments designed to determine atomic positions in solids and interplanar spacings of atoms at surfaces. In such cases, simulation gives more accurate results than any other method. The calculations on atom location have been applied to the experimental results of Swanson and Maury[3] who have shown that, in an Al–0.09 at. % Mn alloy, manganese atoms trap dumbbell interstitials when irradiated at 40 K. Their experiments showed that when an ion beam is scanned through a ⟨011⟩ direction, the dip in scattering from the manganese atoms is much less deep than that for the aluminum atoms and a peak occurs at the center of the dip for the manganese scattering. Computer simulation has been used to study how certain features of the peak and dip depend on the fraction, f_i, of manganese atoms that have trapped interstitials and on the displacement, D, of a trapping atom from its normal lattice site. Two ratios turn out to be of particular interest; these are the ratio (P/V) of the peak at the center of the manganese scan to the valley on either side of it and the ratio (V/S) of the valley to the shoulder region of the scan, which is the region several degrees from the axis where the scattering yield is constant. Table 1.1 shows the dependence of the two ratios on f_i and D. In the table, it can be seen that P/V is a function of D only with no dependence on f_i while V/S is primarily a function of f_i with only a weak dependence on D. Hence, it is possible to measure f_i and D independently of each other. In addition to the values shown in the table, P/V values of 1.43 at $D = 1.45$ Å and 1.51 at $D = 1.50$ Å were calculated for $f_i = 0.6$. From the calculated values together with the experimental value of 1.38, a value of $D = 1.43 \pm 0.05$ Å may be inferred; no result of comparable accuracy is obtainable from any other available theory[3] of channeling. From the results in the lower part of Table 1.1, one could try to estimate the value of f_i. However, the calculated and measured values in the shoulder region differ considerably, so the accuracy of such an estimate would be uncertain. Consequently, no effort has been made to estimate f_i, but the calculations are in reasonable agreement with the value of 0.6 estimated by Swanson and Maury.[3] Absolute values of f_i are probably not of as much interest as absolute values of D, but the changes in f_i during annealing, which are of great interest, can be determined quite accurately.

Table 1.1. Computer simulation results for the backscattering of 1-MeV helium ions from the manganese atoms in Al-Mn interstitials at 35 K

Interstitial fraction	Displacement (Å)			
	1.2	1.4	1.6	1.8
	Peak to valley ratio (P/V)			
0.4	0.98	1.34	1.50	1.94
0.6	0.98	1.34	1.50	1.95
0.8	0.98	1.34	1.50	1.96
	Valley to shoulder ratio (V/S)			
0.4	0.38	0.38	0.40	0.40
0.6	0.60	0.61	0.64	0.65
0.8	0.86	0.87	0.92	0.97

The calculations on surfaces have been applied to the measurements of Davies et al.[4] on the (111) surface of platinum at 40 K. The experimental technique measures the backscattering of incident ions from the surface region of the crystal. At a sufficiently low incident ion energy, the backscattering corresponds to one atom per row. As the incident energy is increased, the scattering rises to a value corresponding to two atoms per row or more. Measurements in the energy range where the scattering is changing rapidly with energy afford a sensitive means of measuring the spacing of the surface layers. Figure 1.9 shows the results of some computer simulations along with the experimental results of Davies et al.; Δd is the deviation of the last interplanar spacing from the value of $d = 2.27$ Å characteristic of the bulk. By comparing the calculated and experimental results, it was estimated that $\Delta d = 0.22 \pm 0.03$ Å. Figure 1.9 also shows some results of a two-atom calculation by Oen.[5] These results diverge from the simulation values in the region of Fig. 1.9 in which more than two atoms make a contribution. However, there is also a large region of the figure in which the two calculations agree, and this region contains two of the three experimental data points. If the two-atom calculation is used with only the two lower energy experimental points, the value of Δd inferred is

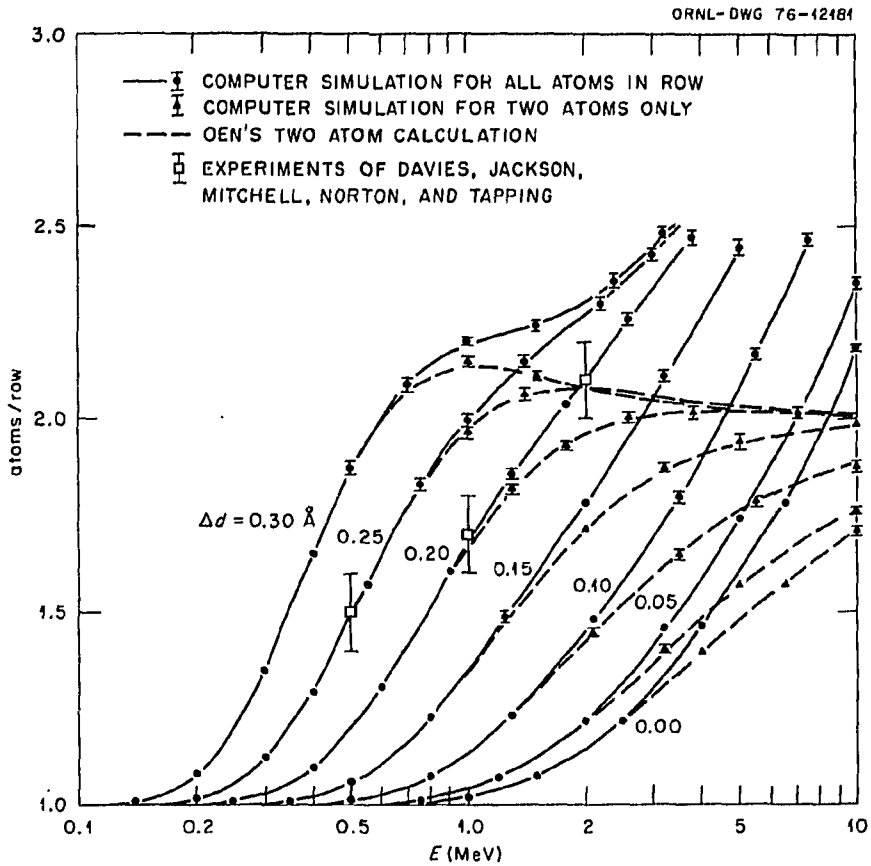

Fig. 1.9. Effective number of atoms per row contributing to backscattering of helium ions incident along [011] onto the Pt(111) surface at 40 K; experimental values are from ref. 4.

virtually the same as given above. Hence both methods are useful.

1. Summary of paper: p. 571 in *Proceedings, Fourth Conference on Scientific and Industrial Applications of Small Accelerators*, ed. by J. L. Duggan and I. L. Morgan. IEEE-76CH1175-9 NTS, Piscataway, N.J., 1977.

2. The methods are summarized in John H. Barrett, *Phys. Rev. B* 3, 1527 (1971).

3. M. L. Swanson and F. Maury, *Can J. Phys.* 53, 1117 (1975).

4. J. A. Davies et al., *Phys. Lett.* 54A, 239 (1975); *Nucl. Instrum. Methods* 132, 609 (1976).

5. O. S. Oen, "Analytical Solutions to the Two-Particle Blocking Model," this report.

ESTIMATIONS OF MINIMUM YIELD FOR CHANNELING

John H. Barrett

The minimum yield for channeling is defined as the ratio of the yield for an ion beam aligned with a major crystallographic direction in a solid to the yield for the beam in a random direction; the ion scattering may be due to large-angle Coulomb scattering or other close encounter processes. There exists a reasonably complete understanding of the axial minimum yield χ^{min} for elemental crystals with clean surfaces.[1,2] However, there are no generally accepted methods for estimating the minimum yield for chemical compounds or for estimating the effect of an amorphous surface layer on the minimum yield. An attempt has been made to develop methods for making these estimates. The attempt has been to generalize the results for elemental solids[2] to give a result in compounds for channeling directions in which all of the atoms in each row are alike. The index 1 will be used to denote the atomic species whose minimum yield is of interest, and $i=2,\ldots,n$ to denote the other species. The generalized result is

$$\chi_1^{min} = C\nu_1\pi\rho_1^2 + C'\pi\sum_{i=2}^{n}\nu_i\rho_i^2 ,$$

where ν_i and ρ_i are the number of rows per unit area and rms thermal vibration amplitude, respectively,

for species i. Values of 3.0 ± 0.3 for C and 1.7 ± 0.2 for C' have been inferred for elements,[2] but the values for compounds may be different. A first test of this result will be made by applying it to the high-T_c superconducting compound V_3Si.

A method to estimate the effect of an amorphous surface layer on the minimum yield was developed on the basis of some computer simulation calculations. Since the available computer program[1] only does simulations for elements, calculations on vanadium were done with and without an amorphous surface layer of specified composition. Because calculations at each temperature used well over an hour of IBM 360/91 time, calculations were done only at 20 K and 298 K, and an attempt was made to generalize the results so as to be usable at other temperatures. The first step in the generalization was to associate the extra yield due to the amorphous layer with the fraction of ions that had been scattered by the amorphous layer at angles greater than some critical value. This critical angle was then associated, by means of the continuum potential of a row of lattice atoms, with a critical distance of approach to the row. Finally, the critical distance of approach was expressed as a multiple of the rms thermal vibration amplitude

$$\rho = \langle x^2 + y^2 \rangle^{1/2} .$$

This is an oversimplified approach, but it is of a type that has often worked well for channeling. The resulting coefficients of ρ were 2.11 ± 0.09 at 20 K and 2.18 ± 0.08 at 298 K, with a resulting average of 2.14 ± 0.06. This appears to be a very promising method for making such estimates, and further calculations will be done to test its generality.

1. J. H. Barrett, *Phys. Rev. B* **3**, 1527 (1971).
2. J. H. Barrett et al., *Radiat. Eff.* **28**, 119 (1976).

EFFECT OF THERMAL VIBRATION AND NUCLEAR RECOIL ON MINIMUM YIELD IN CHANNELING PHENOMENA[1]

J. H. Barrett K. Komaki[2]
F. Fujimoto[2] Y. Hashimoto[2]

From analysis of measurements and computer simulation of channeling, two contributions from thermal vibrations and nuclear lifetime to the axial minimum yield can be distinguished. The first of these is associated with the production of dechanneled trajectories and comes solely from thermal vibrations. It is of the form $C'Nd\pi\rho^2$, where C' is a proportionality constant, N is the number density of crystal atoms, d is the spacing of atoms along the axis, and ρ is the rms amplitude of the components of thermal vibrations normal to the axis. The second contribution is associated with the sampling by lattice atoms of the flux of channeled ions near lattice sites and comes from both thermal vibrations and nuclear lifetime. The form of this contribution is $C''Nd\pi\langle r^2\rangle$, where C'' is a second constant, $\langle r^2\rangle$ is ρ^2 for thermal vibrations and $2(v_\perp \tau)^2$ for nuclear recoil, $v_\perp$ is the component of recoil velocity perpendicular to the axis, and τ is the nuclear lifetime. The combined dependence of the minimum yield χ^{min} on thermal vibrations and nuclear recoil is given by the relation

$$\chi^{min} = Nd[C\rho^2 + 2C''(v_\perp \tau)^2] ,$$

where $C = C' + C''$. From the analysis of measurements and computer simulations, a value of $? \pm 0.3$ was inferred for C and a value of 1.3 ± 0.2 for C''.

1. Summary of paper: *Radiat. Eff.* **28**, 119 (1976).
2. University of Tokyo, Tokyo, Japan.

COMPUTER SIMULATION OF ATOMIC COLLISION CASCADES IN CRYSTALS

M. T. Robinson

The computer simulation program MARLOWE,[1] developed at ORNL over the past several years, is in use here and elsewhere for a variety of calculations of particle ranges, hydrogen reflection, sputtering, and the like.[2,3] It seems appropriate to summarize the many improvements made in the model and in the program recently and to describe the results of some displacement cascade calculations made in copper using the improved model.

The trajectories of particles involved in a displacement cascade are developed in MARLOWE in the binary collision approximation (BCA). The individual scattering events are treated as if they took place between pairs of isolated atoms interacting classically through a conservative central potential. These events are otherwise treated exactly, using numerical quadratures of the classical equations of motion. The program recognizes the occurrence of groups of nearly simultaneous collisions and treats these in a special way: the laboratory momentum of

each target atom is evaluated in the BCA, and the momentum of the projectile is found by applying linear momentum conservation; then, without altering the directions of motion of the particles, their energies are scaled to ensure energy conservation. This procedure gives a much better picture of "simultaneous" collisions than did the original scheme,[1] especially for cases where the particle masses are very different.[4] In addition to these elastic collisions, the program allows for inelastic (electron excitation) energy losses. These losses may be either local (impact parameter dependent), nonlocal, or both. The nonlocal losses were added recently and should allow more realistic calculations of range profiles, especially under channeling conditions.

Several improvements have been made in the model to reduce computing time. The most significant of these was the introduction of a so-called "hash storage" scheme[5] for the lattice sites vacated during cascade development. These sites must be examined at every collision to ensure that vacancies are correctly treated. "Hashing" (in this context) is an associative storing scheme, which assigns a vacated lattice site, not to the next available location, but to a location dependent upon the coordinates of the site in question. It allows the determination of whether or not a site is already in the list of vacant sites in a very rapid manner. A further reduction in time was achieved by an alternative scheme for ordering the collisions. The original method[1] (still an available option) was to follow next the fastest particle currently in the cascade. The new method avoids the list searching implicit in this method by assigning a new priority to a particle whenever its velocity changes. This priority decreases as its velocity decreases. Other improvements involve technical programming details and the pair classification scheme discussed below. The overall result is that the computing time for cascades generated in copper has been reduced by a factor of 2 for 500-eV primaries and by a factor of 12 at 20 keV. The saving is roughly quadratic in energy at higher energies. To reduce storage requirements, the previous a posteriori analysis of replacement sequences has been replaced by one which detects such sequences as they develop. This permits suppression of most replacement events without loss of information and roughly doubles the primary energy which can be reached with a given program size. Furthermore, the program now incorporates a model of the change from mass-transporting replacement sequences to non-mass-transporting focusons. Whenever an apparent replacement event occurs, note is taken of whether the stopped projectile is closer to its own original lattice site or to the replacement site. In the latter case, mass is transported, but in the former, the projectile returns to its own site (if unoccupied).

The atom-site pairs occurring at the end of a cascade can be classified into five groups:

1. Nondisplacements: an atom receives only subthreshold amounts of energy and remains at its own original site. Such atoms are always suppressed.
2. Replacements: a projectile atom occupies (is closely associated with) a lattice site originally occupied by another atom. These atoms may be either preserved or suppressed, as desired.
3. Close pairs: the lattice site nearest to an atom is vacant, but a replacement event did not occur. These pairs are morphologically equivalent to replacements, although they arise by a different series of events.
4. Near pairs: the nearest lattice site is occupied or already paired, but one of its neighboring sites is vacant. In the fcc calculations discussed here, both first- and second-neighbor sites are involved in near pairing.
5. Distant pairs: all other cases.

In the crystalline copper calculations reported below, of all the atoms which enter a cascade, about half terminate their trajectories by replacements, about a third are members of close or near pairs, and the remaining one-sixth are in more distant pairs. The number of atoms receiving subthreshold amounts of energy is much larger than the number of those that enter the cascade. The close and near pairs are regarded as essentially certain to be mechanically unstable and to annihilate athermally.

Cascades have been generated in crystalline copper and in amorphous copper for primary recoil energies ranging up to 22.5 and 25 keV respectively. At the highest energies, sets of 100 cascades were run; more were studied at lower energies. In each case, the Molière potential was used with the screening length deduced before.[1] At each displacement, a binding energy of 0.5 eV had to be overcome. Particles were added to the cascade if they received 5.0 eV in a collision and were considered stopped when their energies fell below 4.5 eV. The purpose of the amorphous calculations was to assess the role of replacement sequences in cascade development. A preliminary analysis of these cascades follows.

In the crystalline calculations, replacement sequences are frequently found. The most important

are ⟨101⟩ sequences which often extend to 25 or more replacements and terminate in focusons when the particle energy falls below about 13 eV. The binding energy employed is sufficient to give approximately the same energy loss rate in these sequences that is found in molecular dynamics calculations.[6] In addition to these sequences, there are appreciable numbers of ⟨001⟩ sequences up to about 13 steps long, somewhat more frequent ⟨111⟩ sequences of up to about 15 steps long, and rare occurrences of ⟨112⟩ sequences of up to five steps. The latter are associated either with primaries moving initially in {111} planes or with the energy losses from ⟨111⟩ sequences.

A significant property of a displacement cascade is the density of defects within it. The cascade *volume* can be defined[7] as the number of lattice sites at which collisions occur. The fraction of these sites vacated is then a measure of the defect density. Figure 1.10 shows this quantity as a function of primary recoil energy for cascades in copper. The *crystalline* results refer to all distant pairs; the *amorphous* to all pairs with separations greater than $a_0 = 3.615$ Å, the cubic cell edge in copper, a value chosen to give roughly the same defect densities as in the crystal case. The density of defects in the amorphous case drops sharply over the energy range up to 70 eV and more slowly thereafter. The initial behavior reflects the increasing cascade volume under circumstances where little multiplication of defects takes place. The behavior of the crystalline calculations is quite different, giving evidence of crystal effects in two different energy regions. These two regions are both connected with replacement collision sequences. As has been described before,[8] collision sequences occurring at low primary recoil energies are mostly initiated directly by the primary particle. At higher energies, they are generated mainly by the much more numerous cascade particles. The two regions are separated by an energy region in which the primary sequences are strongly defocussing, but in which cascade sequences cannot be formed. These two regions are reflected in Fig. 1.10. At recoil energies above about 0.5 keV, the cascade density changes only slowly, in either crystalline or amorphous targets, and becomes sensibly constant above about 12 keV. The persistence of this constancy to even

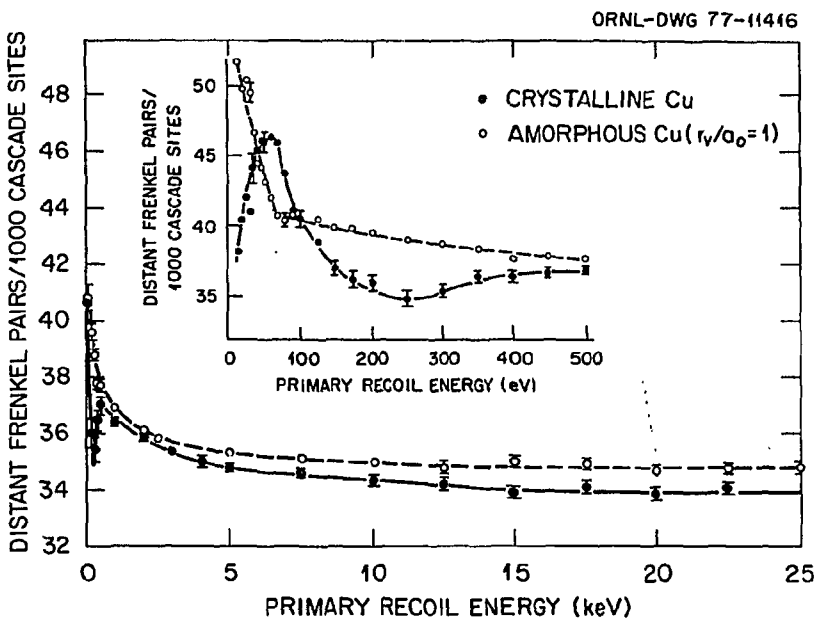

Fig. 1.10. The defect density calculated for cascades in both crystalline and amorphous copper, using the binary collision program MARLOWE.

higher energies will be interesting to explore. Further analyses of these cascades in copper are currently being made.

---

1. M. T. Robinson and I. M. Torrens, *Phys. Rev. B* 9, 5008 (1974).
2. O. S. Oen and M. T. Robinson, "Computer Studies of the Scattering of Low-Energy Hydrogen Ions from Polycrystalline Solid Surfaces," *this report.*
3. J. B. Roberto and M. T. Robinson, "A Measurement of the Transverse Range of $(n,2n)$ Recoils in Gold," this report.
4. M. Hou and M. T. Robinson, *Nucl. Instrum. Methods* 132, 641 (1976).
5. W. D. Maurer and T. G. Lewis, *Comput. Surv.* 7, 5 (1975); D. E. Knuth, *Sci. Am.* 236, 63 (1977); I am indebted to C. A. Coulter of the University of Alabama for first acquainting me with these techniques.
6. D. K. Holmes and M. T. Robinson, *Solid State Div. Annu. Prog. Rep. Dec. 31, 1975*, ORNL-5135, p. 16.
7. J. R. Beeler, Jr., *Phys. Rev.* 150, 470 (1977).
8. D. K. Holmes and M. T. Robinson, p. 225 in *Atomic Collisions in Solids*, vol. 1, ed. by S. Datz, B. R. Appleton, and C. D. Moak, Plenum Press, New York, 1975.

DISPLACEMENT CASCADE LIFETIME IN MONATOMIC SOLIDS

O. S. Oen

In a recent publication, the average time required for an energetic ion or primary knock-on atom (PKA) to slow down to rest in a structureless solid was discussed.[1] This slowing-down time was used to estimate the displacement cascade lifetime, that is, the time elapsed from the moment the PKA receives its initial kinetic energy until the last displaced atom in the cascade comes to rest. A displacement cascade consists of the interstitial atoms and associated vacancies produced when the kinetic energy of a PKA is shared with the lattice atoms. The cascade lifetime is important in treating such problems as thermal spikes[2] and space-time coincidences of displacement cascades.[3]

In this report, a method is presented that enables one to calculate more precisely the displacement cascade lifetime. The basic idea is reminiscent of the solution proposed for the inherent ambiguity in the scattering of indistinguishable particles discussed long ago for the case of α particles in helium.[4] The view is taken that, in elastic collisions in which the striking atom transfers more than one-half of its energy to the struck atom, the identities of the collision partners are interchanged. In other words, the particle emerging with the greater energy following any collision is defined as the "primary" particle. The slowing-down time of this "primary" should be a good measure of the cascade lifetime.

The above physical idea can be formulated mathematically in a straightforward manner. Consider a primary atom of energy E making an elastic collision with a lattice atom. After the collision the primary atom has an energy E' and the lattice atom an energy T, where $E = E' + T$. The differential scattering cross section may be written as

$$\begin{aligned} &d\sigma(E, T)\ ,\ 0 \leqslant T \leqslant E/2\ , \\ &d\sigma(E, E-E')\ ,\ 0 \leqslant E' \leqslant E/2\ . \end{aligned} \tag{1}$$

If we define the "primary" to be that particle emerging with the greater energy following a two-particle collision and replace E' by T, the above cross section becomes

$$d\sigma(E, T) + d\sigma(E, E-T)\ ,\ \ 0 \leqslant T < E/2\ . \tag{2}$$

With this redefined cross section, energy transfers greater than $E/2$ are forbidden. However, the cross section for such events is not simply discarded but rather contributes to an enhancement of the cross section for energy transfers of less than $E/2$.

Given a specific interaction potential and using conventional techniques, one can use Eq. (2) to calculate the slowing-down time and other range quantities of this "primary" as it interacts with the lattice atoms. In the continuous slowing approximation, the mean cascade time is precisely the same as the slowing-down time of the "primary." Figure 1.11 shows the ratio of the mean cascade lifetime to the

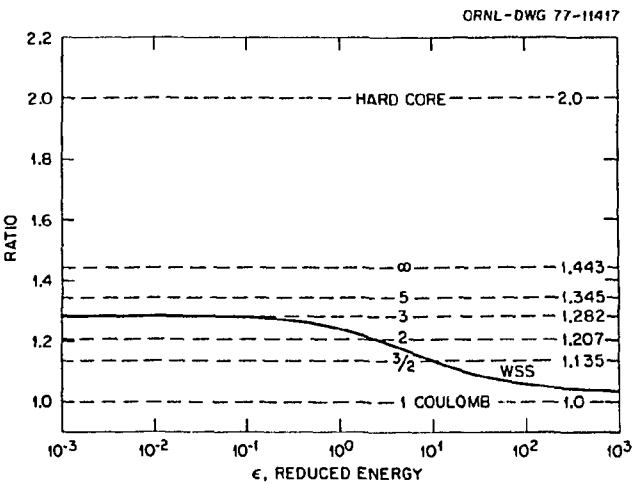

Fig. 1.11. Ratio of cascade lifetime to primary slowing-down time plotted as a function of reduced energy for various power potentials and the Thomas-Fermi potential as approximated by Winterbon, Sigmund, and Sanders (ref. 5).

mean PKA slowing-down time, for several different interaction potentials, as a function of initial PKA energy. The ratio is greater than unity for all potentials except the Coulomb where it is unity. For Thomas-Fermi scattering as approximated by Winterbon, Sigmund, and Sanders (WSS),[5] the mean cascade lifetime at low energies is about 28% larger than the mean PKA slowing-down time, whereas it is just a few percent larger at high energies. The results shown in Fig. 1.11 were obtained assuming no electronic stopping. When electronic stopping is included, the ratio tends to be closer to unity, especially at the larger energies.

In addition to enabling one to calculate mean cascade lifetime and variance, this method of viewing collisions has other interesting applications in radiation damage analysis, such as the interpretation of collision spectra, which are currently being explored.

1. O. S. Oen and M. T. Robinson, *J. Appl. Phys.* 46, 5069 (1975).
2. P. Sigmund, *Appl. Phys. Lett.* 25, 169 (1974).
3. M. T. Robinson, *J. Nucl. Mater.* 53, 201 (1974).
4. E. Rutherford and J. Chadwick, *Philos. Mag.* 4, 605 (1927).
5. K. Winterbon, P. Sigmund, and J. B. Sanders, *K. Dan. Vidensk. Selsk., Mat.-Fys. Medd.* 37, No. 14 (1970).

CALCULATED ENERGY AND ANGULAR DISTRIBUTIONS FOR (*n*,2*n*) RECOILS IN GOLD

J. B. Roberto M. T. Robinson C. Y. Fu[1]

Primary recoil spectra and angular distributions have been computed for (*n*,2*n*) recoils in gold for neutron energies from 10–30 MeV. The kinematics of the (*n*,2*n*) scattering were followed explicitly in a Monte Carlo simulation using theoretical energy distributions for the two emitted neutrons. The calculated recoil energies and angular distributions were used to interpret experimental range measurements[2] for (*n*,2*n*) recoils in gold and to evaluate the effect of multiple particle emissions on recoil energy calculations.

It was assumed that the incident neutrons were inelastically absorbed by the target nuclei and that the two subsequent neutron emissions were isotropic in the barycentric system and independent of each other. The calculated recoil distributions were peaked near the initial energy of the recoiling compound nucleus and at small angles to the incident neutron direction. The widths of the distributions were determined primarily by the first neutron emission. Energy and angular distributions for (*n*,2*n*) recoils resulting from *d*-Be neutron[3] interactions in gold are shown in Fig. 1.12. The corresponding

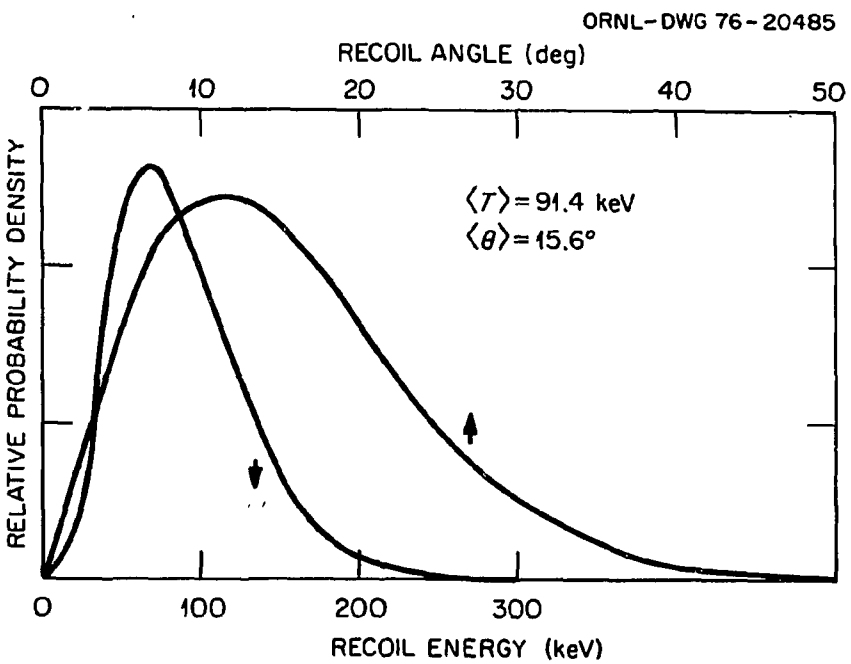

Fig. 1.12. Calculated energy and angular distributions for (*n*,2*n*) recoils resulting from high-energy *d*-Be neutron interactions in gold.

distributions for 15-MeV neutrons in gold are nearly identical to those in Fig. 1.12, since both the *d*-Be spectrum and the Au(n,2n) excitation function are peaked near 15 MeV.

For nonelastic neutron interactions above 15 MeV, it has been assumed[4] that the primary recoil energy can be calculated from the center-of-mass motion and the spectrum of the first emitted light particle. Subsequent particle emissions in reactions such as (n,nx), (n,px), and (n,αx) have been ignored, and the present calculations allow an explicit evaluation of this approximation for the (n,2n) reaction in gold. Over the range of these calculations, the average recoil energy after the second neutron emission was typically 5% greater than the corresponding binary scattering result. This difference is small in comparison with uncertainties in neutron cross sections and therefore supports the use of the binary scattering approximation for the description of nonelastic recoil energies in neutron damage calculations.

1. Neutron Physics Division, ORNL.

2. J. B. Roberto and M. T. Robinson, "A Measurement of the *Transverse Range of* (n,2n) Recoils in Gold," this report.

3. The appropriate *d*-Be spectrum is shown in J. B. Roberto et al., "Damage Production by High-Energy *d*-Be Neutrons in Copper, Niobium, and Platinum at 4.2 K," this report.

4. J. B. Roberto and M. T. Robinson, *J. Nucl. Mater.* 61, 149 (1976).

SPUTTERING CALCULATIONS WITH THE DISCRETE ORDINATES METHOD

T. J. Hoffman[1] D. K. Holmes
H. L. Dodds[1] M. T. Robinson

Hydrogen and helium ions incident on the inner wall of a controlled thermonuclear reactor can sputter atoms from the wall into the plasma, causing erosion of the wall and contamination of the plasma. Sigmund[2] devised a transport model for the calculation of sputtering yields, using an analytical approach to solve the Boltzmann equation. His method is restricted to infinite medium problems in which the differential cross section can be represented by simple analytic expressions. These assumptions are not appropriate to sputtering by light ions.

To treat finite medium problems with arbitrarily complex cross sections, numerical procedures are needed. The most widely used and highly developed method for numerical solution of the Boltzmann equation is the discrete ordinates method.[3] Although the usual application of this method has been to neutron and gamma-ray problems, many of the computational algorithms developed for these problems are applicable to sputtering calculations. The work described here has been directed toward the use of a neutral-particle, discrete ordinates computer code, ANISN,[4] for the calculation of sputtering yields.

A beam of ions is incident on a slab with energy E_s and direction cosine μ_s. A Boltzmann equation can be written for the ions ($i = 1$) and for the target atoms ($i = 2$) that are put into motion by the ions. A multigroup formulation of the problem has been developed, which includes the stopping of the particles by electron excitation, as well as their scattering and multiplication. The sputtering problem is identical to a coupled neutron ($i = 1$) and secondary gamma-ray ($i = 2$) shielding problem with a gamma-ray detector. The discrete ordinates code, ANISN, can solve this type of problem.

Figure 1.13 shows the sputtering yields calculated with ANISN for argon ions incident on copper. In these calculations the differential cross section for the Fermi-Thomas energy range was represented with Winterbon's analytic approximation.[5] For lower energies, Sigmund's power approximation[2] to the Born-Mayer cross section was used. The ANISN results are in good agreement with the experimental data.[6-9] Also shown in Fig. 1.13 are results obtained with the Monte Carlo code, MARLOWE.[10] Unlike ANISN which employs a continuum model of the

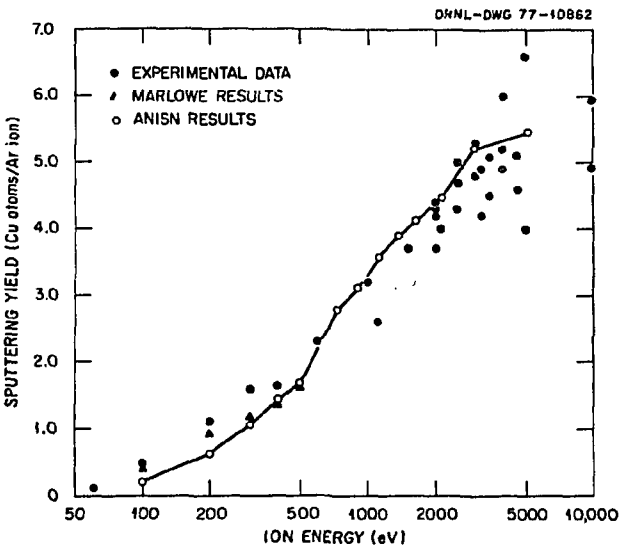

Fig. 1.13. Sputtering yield for argon incident on copper.

target atom structure, MARLOWE uses an atomistic model, but such calculations require considerably more computation time than ANISN calculations. The results shown in Fig. 1.13 indicate that reasonable results can be obtained for this problem without the sophistication and computational expense of the MARLOWE model.

The transport model as presented in this paper has been applied to several sputtering problems. The results obtained thus far indicate that this approach is a viable method for the calculation of sputtering yields.

1. Computer Sciences Division, UCC-ND.
2. P. Sigmund, *Phys. Rev.* **184**, 383 (1969).
3. B. G. Carlson, *Solution of the Transport Equation by the Sn Method*, LA-1891, Los Alamos Scientific Laboratory, Los Alamos, N.M., 1955.
4. W. W. Engle, Jr., *A Users' Manual for ANISN*, K-1693, Oak Ridge National Laboratory, Oak Ridge, Tenn., 1955.
5. K. B. Winterbon, P. Sigmund, and J. B. Sanders, *K. Dan. Vidensk. Selsk., Mat.-Fys. Medd.*, 37, No. 14 (1970).
6. A. L. Southern, W. R. Willis, and M. T. Robinson, *J. Appl. Phys.* 34, 153 (1963).
7. N. Laegreid and G. K. Wehner, *J. Appl. Phys.* 32, 365 (1961).
8. O. Almen and G. Bruce, *Nucl. Instrum. Methods*, 47, 279 (1961).
9. M. I. Guseva, *Fiz. Tverd. Tela* 1, 1540 (1959).
10. M. T. Robinson and I. M. Torrens, *Phys. Rev. B* 9, 5008 (1974).

NEUTRON DAMAGE CALCULATIONS IN COPPER, NIOBIUM, AND GOLD TO 32 MeV: APPLICATION TO SPUTTERING AND DEUTERON-BREAKUP NEUTRON SOURCES[1]

J. B. Roberto M. T. Robinson C. Y. Fu[2]

Primary recoil distributions and specific damage energies have been computed for high-energy deuteron-breakup neutrons in copper, niobium, and gold. The calculations are based on theoretical neutron cross sections and consider in particular a *d*-Be spectrum broadly peaked at 15 MeV with some neutrons above 30 MeV. The theoretical results are similar to corresponding calculations for monoenergetic 15-MeV neutrons and are in good agreement with range measurements of $(n,2n)$ recoils generated by high-energy *d*-Be neutrons in niobium and gold. The calculations are also consistent with recent *d*-Be neutron sputtering experiments in niobium and gold and demonstrate the usefulness of deuteron-breakup neutron sources for simulating fusion neutron effects.

1. Abstract of paper: *J. Nucl. Mater.* **63**, 460 (1976).
2. Neutron Physics Division, ORNL.

THE ENERGY DEPENDENCE OF NEUTRON DAMAGE IN COPPER AND NIOBIUM[1]

J. B. Roberto M. T. Robinson

Primary recoil spectra and specific damage energies have been computed for neutron interactions in copper and niobium at neutron energies up to 32 MeV. The calculations are based on theoretical neutron cross sections and are in good agreement with recent radiation damage experiments using high-energy neutrons from the Be(d,n) reaction. The results are particularly relevant to the understanding of radiation effects from high-energy deuteron-breakup neutron sources.

1. Abstract of paper: *J. Nucl. Mater.* **61**, 149 (1976).

APPROXIMATIONS FOR SIMPLE DEFECT KINETIC EQUATIONS

G. Leibfried[1] D. K. Holmes

The Low-Temperature Irradiation Group of the Solid State Division has recently irradiated very pure copper crystals at room temperature in the Bulk Shielding Reactor (CP-15 facility) of ORNL.[2] The work presented here was stimulated by an attempt to analyze their data using appropriate rate equations.

At a temperature of the order of 330 K both vacancies and interstitials and, possibly, divacancies and di-interstitials, are mobile. The processes that must be considered are mutual annihilation, disappearance at unsaturable sinks, trapping, and clustering. The rate equations that include these events are nonlinear and require careful treatment in computer calculations to avoid instabilities in the solution. It is of interest to consider analytic approximations to the simpler forms of such equations. For very early irradiation times, it is expected that vacancy-interstitial annihilation and disappearance at unsaturable sinks will be the dominant processes, at least in some cases. The following equations for the interstitial and vacancy

concentrations represent a very simple approach to the early time behavior:

$$\frac{di}{dt} = 1 - iv - \alpha i \,, \tag{1a}$$

$$\frac{dv}{dt} = 1 - iv - \beta v \,. \tag{1b}$$

The following definitions hold:

$$i = \gamma I \,, \quad v = \gamma V \,,$$

where I and V are the atomic concentrations of interstitials and vacancies respectively;

$$\gamma = \sqrt{\nu_i \lambda_i \sigma_{iv} / p} \,,$$

where

ν_i is the jumping rate for interstitials,

λ_i is the jump distance,

σ_{iv} is the *effective* pair annihilation cross section,

λ_i and σ_{iv} are in units of the lattice parameter,

p is the production rate for vacancies and interstitials per atom per second;

$$\nu_i \cong \nu_0 \exp(-E_i/kT) \,,$$

where

$\nu_0 \sim 10^{13}$ sec^{-1},

E_i is the activation energy for motion of the interstitials;

$$t = \tau \sqrt{p \nu_i \lambda_i \sigma_{iv}} \,,$$

where τ is the irradiation time in seconds;

$$\alpha = \gamma (\sigma_{is}/\sigma_{iv}) S_i \,,$$

$$\beta = (\gamma_v^2/\gamma)(\sigma_{vs}/\sigma_{iv}) S_v \,.$$

$$\gamma_v = \sqrt{\nu_v \lambda_v \sigma_{iv} / p} \,,$$

where σ_{is} and σ_{vs} are the *effective* capture cross sections of unsaturable sinks for interstitials and vacancies, respectively, and S_i and S_v are the atomic concentrations of the sinks. From the definitions, it can be seen that α and β may vary over many orders of magnitude, depending on the irradiation conditions. The treatment to be discussed here assumes that β is very much smaller than α because of the much lower mobility of the vacancies. Taking the initial condition to be

$$i(0) = v(0) = 0 \text{ at } t = 0 \,, \tag{2}$$

the first area of interest is for small values of t, for which the term βv may be neglected.

Even this set of simplified, nonlinear equations does not have a complete, explicit, analytical solution, so that numerical integration is the obvious method of treatment. However, it is possible to derive some worthwhile approximations. The principal feature of the short time behavior is that, while the vacancy concentration rises monotonically, the interstitial concentration goes through a maximum. The goal here is to find approximate values for the time, t_M, to reach the maximum interstitial concentration, along with approximate forms for the concentrations at times through t_M.

Ignoring the βv term, the scheme for developing early time forms is

1. *for small* α, obtain zeroth-order expressions (i_0 and v_0) by neglecting the αi term; better approximations are then obtained by treating the αi term as a perturbation;

2. *for large* α, drop the iv term in Eq. (1*a*), and then use it as a perturbation.

The results from this approach are the following.

For small α:

$$\left.\begin{matrix} i \\ v \end{matrix}\right\} = \tanh t - [\alpha(\tanh^2 t)/4] \mp [\alpha \ln(\cosh t)/2] \,, \tag{3a}$$

$$t_M \cong \ln\sqrt{8/\alpha} \,, \quad (\text{error} < 10\%, \text{ for } \alpha \leqslant 0.3). \tag{3b}$$

For large α:

$$i = \alpha^{-1}[1 - \exp(-\alpha t)] - f' \,, \tag{4a}$$

$$v = \alpha[1 - \exp(-t/\alpha)] + f' \,, \tag{4b}$$

$$f' = \alpha^{-1} - (\alpha - 2/\alpha)^{-1}\exp(-t/\alpha) + 2\alpha^{-2}(\alpha - 2/\alpha)^{-1}\exp(-\alpha t/2) \,, \tag{4c}$$

$$t_M \cong (2 \ln \alpha)/\alpha \,, \text{ (error} < 10\%, \text{ for } \alpha \geqslant 4.0) \,. \tag{4d}$$

In each case, values at the maximum correspond to setting

$$\left.\frac{di}{dt}\right|_{t_M} = 0 . \tag{5}$$

The resulting formulas are transcendental and not readily soluble. The forms for t_M given in Eqs. (3) and (4) are further approximations to the more accurate equations resulting from the use of Eq. (5). As α decreases, Eq. (3*b*) becomes more and more accurate—and essentially becomes exact for $\alpha \leqslant 0.01$. Similarly for large α, Eq. (4*d*) is effectively exact for $\alpha \geqslant 20$.

In the range $0.3 \leqslant \alpha \leqslant 4.0$, the functional form of $t_M(\alpha)$ is very well represented by the interpolation formula:

$$t_M = \begin{cases} (2 \ln \alpha)/\alpha , & \alpha \geqslant 8 , \quad (6a) \\ \ln\sqrt{8/\alpha} + 0.52(\alpha/8)^n , & \alpha \leqslant 8 , \quad (6b) \end{cases}$$

where $n \cong 2.318447$.

For all values of α, the interstitial concentration falls off very slowly with irradiation time after t_M, as has been previously observed.[3,4] For times somewhat larger than t_M,

$$i \cong (v + \alpha)^{-1} , \tag{7}$$

so that

$$\frac{dv}{dt} = \alpha(v + \alpha)^{-1} - \beta v . \tag{8}$$

If the βv term is taken to represent the approximate size of all terms which involve vacancy migration and if $\beta \ll 1$, then the further approximation

$$\frac{dv}{dt} = \alpha(v + \alpha)^{-1} \tag{9}$$

will apply until the two terms on the right-hand side of Eq. (8) are roughly equal. Such considerations may be of help in starting the numerical integration of the much more complicated set of equations which more realistically represents the behavior of the defects during irradiation.

In the case of the irradiation of copper at room temperature, values of α and β may be of the order of 10^3 and 10^{-6} respectively, using activation energies of motion of 0.12 eV for interstitials and 0.71 eV for vacancies. These values lead to the result that the mobile interstitial concentration passes through its maximum at a very small fraction of a second of irradiation time. Further, within a very few seconds the processes due to vacancy migration would become of importance. This indicates that for experimentally significant irradiation times the interstitial concentration may be well represented by an expression of the type of Eq. (7), obtained by setting

$$\frac{di}{dt} \cong 0 .$$

The resultant form for $i(t)$ can then be used in all other equations of the complete set.

---

1. Consultant from Institut für Festkorperförschung, Kernforschungsanlage, Jülich, Germany.

2. R. L. Chaplin et al., "Defect and Transmutation Resistivity in Reactor-Irradiated Copper," this report.

3. G. J. Dienes and A. C. Damask, *Phys. Rev.* 128, 2542 (1962).

4. J. V. Sharp and A.J.E. Foreman, *Calculation of Build-Up Times for Radiation Enhanced Diffusion*, AERE-R5786, Great Britain Atomic Energy Research Establishment, Harwell, Berks, England, June 1968.

ELECTRONIC AND MAGNETIC PROPERTIES

CLUSTER CALCULATIONS: SIMULATION OF BULK PROPERTIES

Mark Mostoller Theodore Kaplan

Calculations in which the essentially infinite number of atoms in a real solid is replaced by a large, but finite, number of atoms have been used for some time to simulate a variety of material properties. A familiar example of these so-called "cluster calculations" is the molecular dynamics or equation-of-motion approach, which has been used to study the behavior of liquids, phase transitions, the electronic density of states of alloys, and a large number of other problems. We have been exploring variations of another approach to large cluster calculations which shows promise of similarly broad applications.

Specifically, we have been investigating methods based on the Lanczos algorithm[1] for tri-diagonalizing matrices. Suppose, for example, that we wish to determine the local electronic density of states in a

solid described by a one-band, nearest-neighbor, tight-binding Hamiltonian,

$$H = \sum_i e_i |i\rangle\langle i| + \sum_{i,j} t(i, j)|i\rangle\langle j| . \quad (1)$$

Here e_i is the site-diagonal energy for an electron at site i, and $t(i, j)$ is the transfer or hopping integral connecting sites i and j. The density of states at site 1 as a function of energy E can be expressed in terms of the (1, 1) element of the inverse matrix $(E - H)^{-1}$,

$$\rho_1(E) = -\frac{1}{\pi} \operatorname{Im} \lim_{\delta \to 0} \langle 1|[(E + i\delta) - H]^{-1}|1\rangle . \quad (2)$$

Starting with the vector $|v_1\rangle = |1\rangle$, the Lanczos algorithm generates an orthonormal set of vectors $|v_k\rangle$ according to the following prescription:

$$\beta_{k+1}|v_{k+1}\rangle = (H - \alpha_k)|v_k\rangle - \beta_k|v_{k-1}\rangle , \quad (3a)$$

$$\alpha_k = \langle v_k| H |v_k\rangle , \quad (3b)$$

β_{k+1} specified such that $\langle v_{k+1}|v_{k+1}\rangle = 1$. (3c)

In terms of these vectors, the Hamiltonian H is tri-diagonal, that is,

$$\langle v_{k+l}| H|v_k\rangle = \langle v_k| H|v_{k+l}\rangle = \alpha_k\delta(l, 0) + \beta_{k+1}\delta(l, 1) , \quad (4a)$$

$$\langle v_{k+l}| H|v_k\rangle = \langle v_k| H|v_{k+l}\rangle = 0 , \quad l > 1 . \quad (4b)$$

With H in tri-diagonal form, the (1, 1) element of the inverse matrix $(z - H)^{-1}$ can be written as a continued fraction,

$$\langle 1|(z - H)^{-1}|1\rangle = 1/(z - \alpha_1 - \beta_2^2/z - \alpha_2 - \beta_3^2/z - \ldots) . \quad (5)$$

The local density of states can now be found by combining Eqs. (2) and (5).

For electrons in the bulk of a solid, the right-hand side of Eq. (5) is an infinite continued fraction. To simulate bulk properties, we apply a recursion method similar to that proposed by Haydock, Heine, and Kelly.[2] Some number of the coefficients α_k, β_{k+1} are determined by application of the Lanczos algorithm, Eqs. (3a)-(3c), to a large cluster of atoms, and the lower end of the continued fraction is replaced by some function $g_\infty(z)$ which has certain desired properties, for example, the correct bandwidth. In Figs. 1.14 and 1.15, electronic and phonon densities of states calculated by the recursion method are compared to exact results. In each case, recursion was

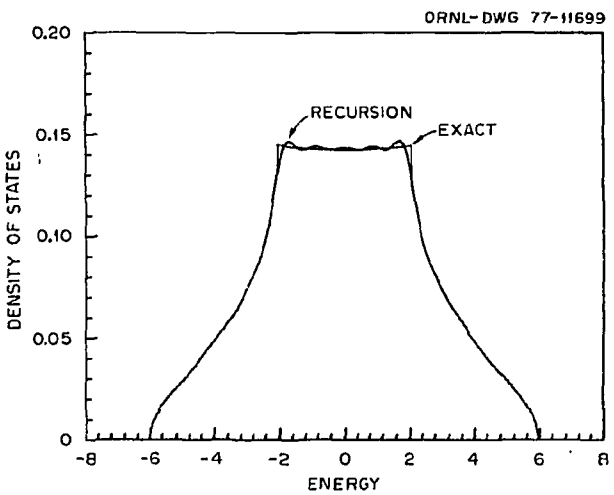

Fig. 1.14. Density of states for s electrons in a simple cubic lattice with first-nearest-neighbor interactions, as calculated by the recursion method, compared to the exact results. Recursion was applied after level 21 in a 22-level lattice of 13,287 atoms.

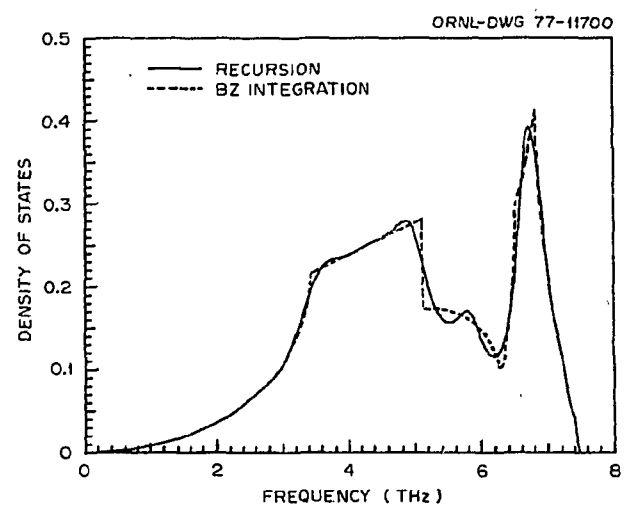

Fig. 1.15. Phonon density of states in copper with first-nearest-neighbor interactions, as calculated by the recursion method and by Brillouin zone integration. Recursion was applied after level 11 in a 12-level lattice of 5083 atoms.

applied to quite large clusters one level before the Lanczos algorithm reached the cluster boundary.

Figures 1.14 and 1.15 show that a simple recursion procedure gives good results for pure bulk materials. Similarly good results can be anticipated for isolated defects in pure materials and for surface vibrations and electronic states; recursion calculations of surface vibrations are described in another contribution to this annual report.[3] For alloys, however, the simple recursion procedure used to obtain Figs. 1.14 and 1.15 does not give acceptable results. Alloy densities of states determined by this simple method exhibit structure that depends upon the recursion level in a nontrivial way. Studies of more sophisticated recursion procedures for alloys are in progress.

1. J. H. Wilkinson, *The Algebraic Eigenvalue Problem*, Clarendon Press, Oxford, 1975.

2. R. Haydock, V. Heine, and M. J. Kelly, *J. Phys. C* 8, 2591 (1975).

3. Mark Mostoller and Theodore Kaplan, "Lattice Vibrations at Surfaces," this report.

DISORDERED SYSTEMS WITH SHORT-RANGE ORDER[1]

Theodore Kaplan L. J. Gray[2]

Previously we described a theory for elementary excitations in random substitutional alloys.[3] This theory correctly treats off-diagonal as well as diagonal disorder, and it generates translationally invariant, analytic Green functions which are valid for excitations in all mean-free-path regions. The theory is based upon a technique for averaging functions of independent random variables which was introduced by Mookerjee.[4,5]

Disordered systems with short-range order, which include many alloys, amorphous solids, and liquids, can only be described in terms of dependent random variables. Because this averaging formalism is restricted to considering only functions of independent random variables, it cannot be applied to disordered systems with short-range order. Here, we show how the averaging formalism can be generalized to include functions of dependent random variables and thus obtain a general theory for elementary excitations in disordered systems. We call this averaging technique the Augmented Space Formalism (ASF).

The inclusion of dependent random variables into the theory does not alter the basic concept. As before, rather than averaging the real-space Green function directly, we construct a new, nonrandom Hamiltonian defined on the much larger augmented space. This new space can be described as the direct product of the Hilbert space spanned by the original Hamiltonian with a "disorder" space which accounts for the allowed configurations of the disordered system. The new Hamiltonian is defined such that configurational averages in real space are equal to inner products in augmented space. The inner products can then be approximated by any one of several methods.[4,6,7]

To be specific, we consider the electronic properties of a random, binary A-B alloy with short-range order. The configuration of the alloy is described in terms of site occupation variables $\{s_i\}$, where $s_i = s_A$ (s_B) if an A atom (B atom) is present at site i. For alloys with short-range order, the s_i are not independent.

In a disordered system it is the configurationally averaged properties that are of physical interest. For the Hamiltonian H, the configurationally averaged Green function is given by the relation

$$\bar{G}_{ij}(z) = \int\int\cdots\int \langle\psi_i|[zI - H(\{s_k\})]^{-1}|\psi_j\rangle\, P(\{s_k\}) \prod_{n=1}^{\infty} ds_n \,. \tag{1}$$

H is defined on the Hilbert space Ω, $\{\psi_i\}$ is a set of basis vectors in Ω, and P is the joint probability density function for the disordered system.

In order to construct an inner product in augmented space which is equivalent to configurational averaging in real space, we first decompose P into a product of conditional probability densities:

$$P(s_1, s_2, s_3, \ldots) = p_1(s_1)p_2(s_2/s_1)p_3(s_3/s_1, s_2)\ldots . \tag{2}$$

For any joint probability distribution, such a decomposition is always possible. For the conditional densities $p_j(s_j/s_1, s_2, \ldots s_{j-1})$, we construct a Hilbert space ϕ_j and a unit vector v_j^0 in ϕ_j. For a binary alloy, ϕ_j is two-dimensional. A "disorder" space Φ and a unit vector γ_0 in Φ are then defined as the direct products of the ϕ_j and the v_j^0, respectively, that is,

$$\Phi = \bigotimes_{i=1}^{\infty} \phi_i \,, \quad \gamma_0 = \bigotimes_{i=1}^{\infty} v_i^0 \,, \tag{3}$$

where $\otimes$ denotes the direct or tensor product. To each random variable s_j we assign a self-adjoint operator $\tilde{S}_j$ acting on Φ such that $\{\tilde{S}_j\}$ form a commuting set. To

define $\tilde{S}_j$ we proceed as follows: for each space ϕ_j and vector v_j^0 select self-adjoint operators $M_j^{\alpha_1,\alpha_2,\ldots,\alpha_{j-1}}$ on ϕ_j such that

$$p_j(s_j/s_1 = s_{\alpha_1}, s_2 = s_{\alpha_2}, \ldots, s_{j-1} = s_{\alpha_{j-1}}) = -\frac{1}{\pi}\lim_{s\to s_j+i0} \operatorname{Im}\langle v_j^0|(sI_j - M_j^{\alpha_1,\alpha_2,\ldots,\alpha_{j-1}})^{-1}|v_j^0\rangle , \tag{4}$$

where α_i = A or B and I_j is the identity operator defined in ϕ_j. For a binary alloy, the M_j are 2×2 matrices; several examples of the construction of these M matrices are discussed by Mookerjee.[4] We can now set

$$\tilde{S}_1 = M_1 \otimes I_2 \otimes I_3 \otimes \ldots$$

$$\tilde{S}_2 = \sum_{\alpha_1=A}^{B} \delta(M_1, s_{\alpha_1} I_1) \otimes M_2^{\alpha_1} \otimes I_3 \otimes I_4 \otimes \ldots$$

$$\tilde{S}_3 = \sum_{\alpha_2=A}^{B}\sum_{\alpha_1=A}^{B} \delta(M, s_{\alpha_1} I_1) \otimes \delta(M_2^{\alpha_1}, s_{\alpha_2} I_2) \otimes M_3^{\alpha_1,\alpha_2} \otimes I_4 \ldots \tag{5}$$

$$\vdots$$

$$\tilde{S}_k = \sum_{\alpha_{k-1}=A}^{B} \cdots \sum_{\alpha_1=A}^{B} \delta(M_1, s_{\alpha_1} I_1) \otimes \ldots \otimes \delta(M_{k-1}^{\alpha_1,\ldots,\alpha_{k-2}}, s_{\alpha_{k-1}} I_{k-1}) \otimes M_k^{\alpha_1,\ldots,\alpha_{k-1}} \otimes I_{k+1} \ldots$$

$$\vdots$$

where $\delta(M, sI)$ is the Kronecker delta function. $\delta(M_j^{\alpha_1,\ldots,\alpha_{j-1}}, s_\lambda I_j)$ is the projection operator onto the eigenvector with eigenvalue s_λ in the space ϕ_j. The operator $\delta(M_1, s_{\alpha_1} I_1) \otimes \ldots \otimes \delta(M_j^{\alpha_1,\ldots,\alpha_{j-1}}, s_{\alpha_j} I_j)$ represents the configuration $s_1 = s_{\alpha_1}, \ldots, s_j = s_{\alpha_j}$ and assigns to it the appropriate probability. A discussion of the construction of the matrix representation of such delta functions is given by Kaplan and Gray.[3] We note that if the s_i are independent this reduces to the form originally given by Mookerjee.[4]

We can now define the augmented space $\Sigma = \Omega \otimes \Phi$ and a nonrandom Hamiltonian $\tilde{H} = H(\{\tilde{S}_i\})$ which is defined on Σ. The configurationally averaged Green function is then given by the inner product in augmented space

$$\overline{G}_{ij}(z) = \langle \psi_i \otimes \gamma_0 | (zI_\Sigma - \tilde{H})^{-1} | \psi_j \otimes \gamma_0 \rangle , \tag{6}$$

where I_Σ is the identity operator on Σ. All the physical and statistical information about the alloy is now contained in $\tilde{H}$.

We note that Mookerjee's original derivation of the averaging formalism is based upon the independence of the random variables. However, by considering $\{s_i\}$ as defining a distribution on a Hilbert space,[8] it can be seen that the independence of the $\{s_i\}$ is not crucial. Mathematical details will appear elsewhere.

To calculate the inner product given in Eq. (6), one may employ any suitable approximation technique. The recursion method of Haydock, Heine, and Kelly[9] and the graphical method of Anderson[10] have received the most attention so far in treating such inner products.

As an illustrative example of the use of the ASF we have investigated the simplest solid with short-range order—a one-dimensional binary A–B alloy whose configurations are determined by a first-order Markov process.[11] We have used the conventional nearest-neighbor, tight-binding Hamiltonian to describe the electronic properties of the alloy:

$$H_{ij} = e(s_i)\,\delta_{ij} + W_{ij} ,$$

$$e(s_i) = e_A\,\delta(s_i, s_A) + e_B\,\delta(s_i, s_B) ,$$

$$W_{ij} = \begin{cases} W & |i-j| = 1 , \\ 0 & \text{otherwise,} \end{cases} \tag{7}$$

where $H_{ij} = \langle \psi_i | H | \psi_j \rangle$. In a first-order Markov chain, the configurations of the system are determined by the transition probability matrix

$$t = \begin{bmatrix} t_{AA} & t_{AB} \\ t_{BA} & t_{BB} \end{bmatrix} \tag{8}$$

where $t_{\alpha\beta} = p(s_k = s_\beta / s_{k-1} = s_\alpha)$ is the probability of finding an atom of type β at site k given there is an atom of type α at site $k-1$. Painter and Hartmann[11] have shown that, for a chain composed of A and B atoms, the Markov system can be completely specified by the fraction of B atoms in the chain, c_B, and the t_{BB} element of the transition probability matrix.

Using the augmented space formalism and the recursion method of Haydock, Heine, and Kelly,[9] we have calculated the density of states of Markov chains with $e_A = 3.0$, $e_B = -3.0$, $W = 1.0$, and $c_B = 0.5$. In Figs. 1.16–1.17, the densities of states for chains calculated using the ASF and a recursion level of 8 are compared with essentially exact results obtained using the Schmidt[12] method on chains of 100,000 atoms for $t_{BB} = 0.1$ and 0.9 respectively. Since the

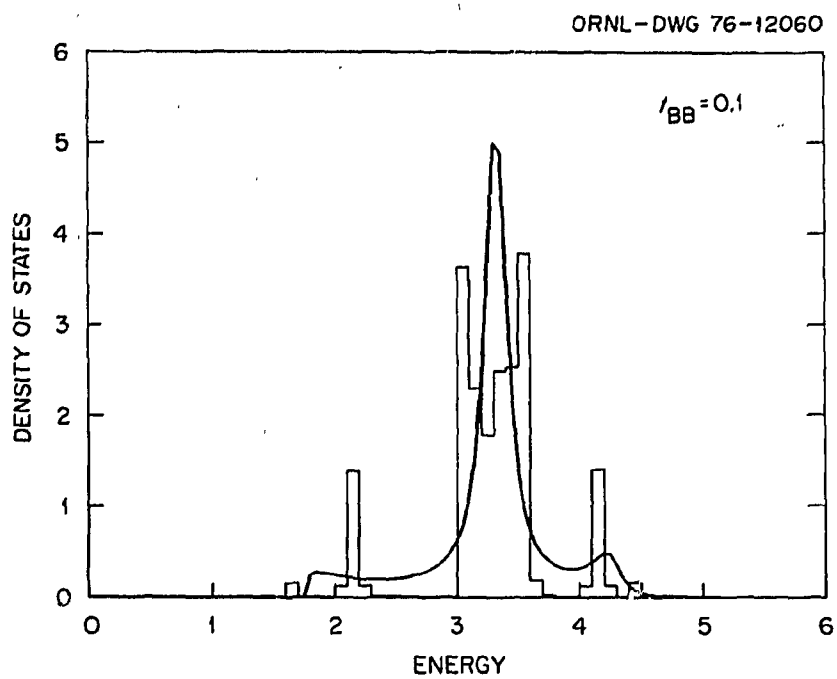

Fig. 1.16. Comparison of the density of states calculated in the ASF with a recursion level of 8 (smooth curve) with the corresponding exact calculation (histogram) for a 100,000 atom chain. The parameters of the one-dimensional electronic alloy are $e_A = -e_B = 3.0$, $W = 1.0$, $c_B = 0.5$, and $t_{BB} = 0.1$.

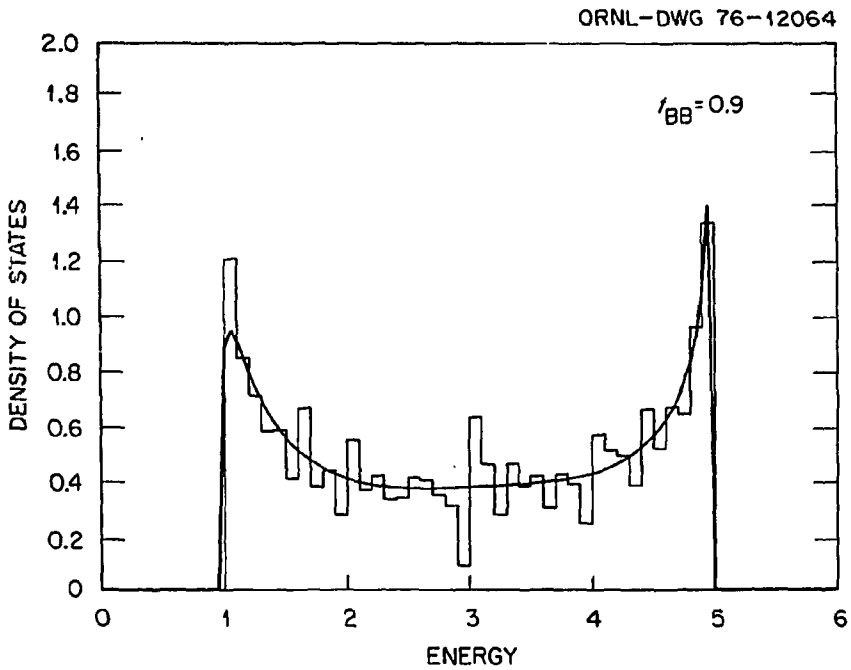

Fig. 1.17. Density of states with $t_{BB} = 0.9$ and all other parameters the same as in Fig. 1.16.

distributions are symmetric about zero for $c_B = 0.5$, we have plotted the results for positive energies only. The theory agrees reasonably well with the exact results throughout the entire energy spectrum. The theory correctly predicts the bandwidth and the major peaks in the density of states. For t_{BB} small, like atoms tend not to be near one another, and the resulting structure in the density of states is very sharp. As $t_{BB} \to 1$, the density of states reduces to the sum of two independent bands, one for the A atoms and one for the B atoms.

1. Summary of papers: *J. Phys. C* 9, 1483 (1976); *Phys. Rev. B* 15, 3260 (1977).
2. Computer Sciences Division, UCC-ND.
3. T. Kaplan and L. J. Gray, *J. Phys. C* 9, 1303 (1976).
4. A. Mookerjee, *J. Phys. C* 6, 1340 (1973).
5. A. Mookerjee, *J. Phys. C* 6, 1202 (1973).
6. A. Mookerjee, *J. Phys. C* 8, 20 (1975).
7. A. R. Bishop and A. Mookerjee, *J. Phys. C* 7, 2165 (1974).
8. L. Gross, p. 51 in *Analysis in Function Space*, ed. by W. T. Martin and I. Segal, MIT Press, Cambridge, Mass., 1963.
9. R. Haydock, V. Heine, and M. J. Kelly, *J. Phys. C* 8, 2591 (1975).
10. P. W. Anderson, *Phys. Rev.* 109, 1492 (1958).
11. R. D. Painter and W. M. Hartmann, *Phys. Rev. B* 10, 2159 (1974).
12. H. Schmidt, *Phys. Rev.* 105, 425 (1957).

SPECTRAL FUNCTIONS OF DISORDERED SYSTEMS

Theodore Kaplan L. J. Gray[1]

In the interpretation of many experiments, spectral functions must be calculated in order to understand the result properly. For example, in neutron scattering experiments the inelastic cross section is related to the spectral function of a displacement-displacement Green's function.

Using the Augmented Space Formalism (ASF),[2,3] we can express the spectral function of a disordered system as a diagonal element of a new nonrandom operator. The ASF is particularly well suited for this purpose, since it automatically includes the translational invariance which results from averaging over all configurations of the disordered system. We approximate this matrix element by using the recursion method,[4] a method which guarantees analyticity. Because our approximation is based on the ASF, it is quite general and can include both diagonal and off-diagonal disorder, multisite correlations, and short-range order.

Model calculations have been completed for the spectral function of the electron one-particle propagator of a three-dimensional simple cubic A-B alloy with a nearest-neighbor, tight-binding Hamiltonian. In Figs. 1.18 and 1.19 the results of this approximation are compared with cluster calculations of Alben,

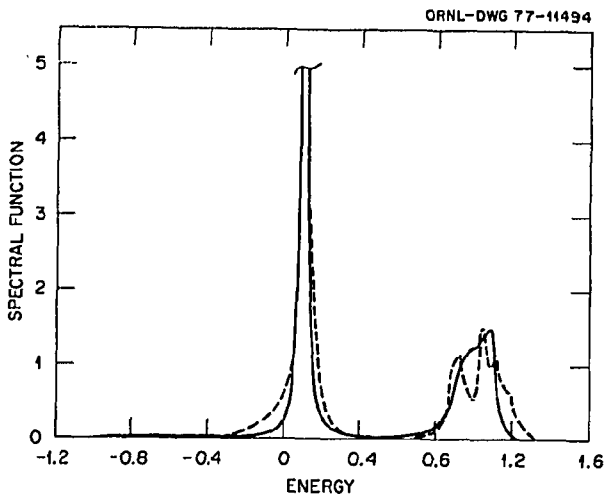

Fig. 1.18. Comparison of the spectral function of a diagonally disordered alloy calculated by the ASF method (solid curve) and by a cluster method (dashed curve).

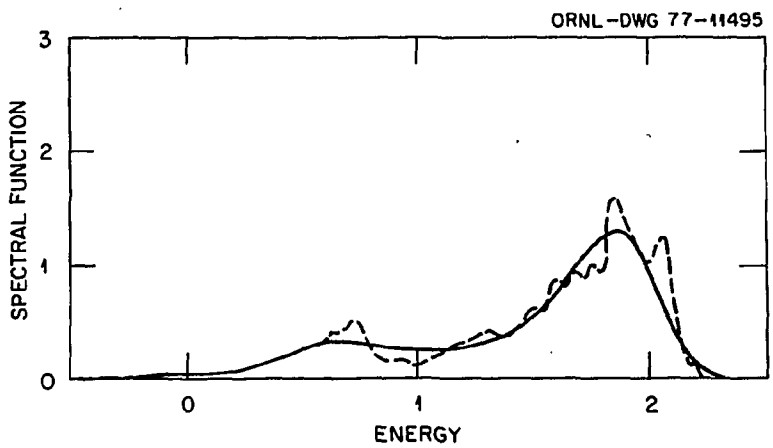

Fig. 1.19. Comparison of the spectral function of an off-diagonally disordered alloy calculated by the ASF method (solid curve) and by a cluster method (dashed curve).

Krakauer, and Schwartz[5] for a diagonally disordered and an off-diagonally disordered alloy, respectively, at the reciprocal lattice vector (0, 0, 0). The overall agreement is quite good in both cases.

1. Computer Sciences Division, UCC-ND.
2. T. Kaplan and L. J. Gray, *Phys. Rev. B* 14, 3462 (1976).
3. T. Kaplan and L. J. Gray, *Phys. Rev. B* 15, 3260 (1977).
4. R. Haydock, V. Heine, and M. J. Kelly, *J. Phys. C* 8, 2591 (1975).
5. R. Alben, H. Krakauer, and L. Schwartz, *Phys. Rev. B* 14, 1510 (1976).

ELECTRONIC STRUCTURE OF TRAPPED-HOLE CENTERS IN MgO

T. M. Wilson R. F. Wood

The ground state of the V^- center[1] in the alkaline-earth oxides consists of a hole trapped on an oxygen ion by a nearest-neighbor cation vacancy. Hence there is an O^- ion instead of an O^{2-} ion at the trapping site. Both spin resonance and optical absorption have been detected for this defect in MgO, CaO, and SrO. The localization of the hole appears to be the result of, or at least aided by, self-induced lattice distortions. The hole can be thermally transferred between the oxygen ions immediately adjacent to the vacancy, but the hopping frequency is relatively low compared to the characteristic time of lattice vibrations. Many of the properties of the V^- center can be understood qualitatively on the basis of a simple ionic model according to which the threefold degeneracy of the O^- $2p$ free-ion energy level is split by the axially symmetric field of the cation vacancy. This splitting can be used to interpret the optical absorption, provided the polarization of the O^- orbitals by the vacancy is taken into account. This model has been criticized by Schirmer, Koidl, and Reik,[2] who have proposed an alternate model based on small polaron theory. It seems likely that a complete description of the V^- center will involve elements of both models.[3]

We have developed an approach to the ionic model based on methods used previously to calculate the electronic structure of lattice defects in the alkaline-earth oxides and alkali halides. We explicitly treat the Coulomb and exchange interactions between the orbitals on the O^- ion and those on the neighboring ions, and we include electronic and ionic polarization effects as well as lattice distortions. The calculation of the electronic structure of the O^- ion itself is carried out using the self-consistent, open-shell Hartree-Fock-Roothaan procedure.[4] At this time, we have calculated the orbitals of the O^- ion embedded in the crystal with two different basis sets of one-electron functions and with the ions frozen in their perfect lattice positions. The most flexible basis set has $2(1s)$, $2(2s)$, $2(3s)$, $2(2p)$ and $2(3p)$ Slater-type orbitals (STO's) to describe the σ orbital[5] manifold and $5(2p)$ STO's for the π orbitals.[5] We found that the 1σ orbital is essentially identical to the O^- $1s$ orbital. The 2σ orbital is highly polarized away from and the 3σ is slightly polarized towards the Mg^{2+} vacancy. In both the 2σ and 3σ orbitals, there is significant s-p orbital mixing. Such effects should be extremely important in determining the transition energies and oscillator strengths, and such ground state properties as ENDOR and EPR result. Further calculations of the excited states are in progress and will be used to interpret the experimental data for both the V^- center and the $[Li]^0$ center, which is discussed elsewhere[6] in this report.

1. Other trapped-hole centers are formed when light-element impurity ions replace the cation; for example, the $[Li]^0$ center in MgO consists of a hole on the O^- ion trapped by a substitutional Li^+ ion at a normal Mg^{2+} site.
2. O. F. Schirmer, P. Koidl, and H. G. Reik, *Phys. Status Solidi B* 62, 385 (1974).
3. M. J. Norgett, A. M. Stoneham, and A. P. Pathak, *J. Phys. C* 10, 555 (1977).
4. C.C.J. Roothaan and P. S. Bagus, p. 47 in *Methods in Computational Physics*, vol. 2, ed. by B. Alder, S. Fernback, and M. Rothenberg, Academic Press, New York, 1963.
5. The $1s$ and $2s$ orbitals and the $2p$ orbital directed toward the cation vacancy go over into σ orbitals in the axially symmetric field of the vacancy; the $2p$ orbitals perpendicular to the vacancy $-O$ ion axis go over into π orbitals.
6. F. A. Modine, "Magneto-Optical Properties of $[Li]^0$ Defects in MgO," this report.

FIRST-PRINCIPLES INVESTIGATION OF THE EXCHANGE INTERACTION IN THE HEAVY RARE EARTHS

J. F. Cooke

The wide variety of magnetic behavior which has been observed in the heavy rare earth series can be adequately described in terms of a localized spin model consisting of an exchange interaction, $J(\mathbf{q})$, between spins on different sites and a crystal field whose lowest lying levels belong to a specific spin multiplet. According to the RKKY (Ruderman, Kittel, Kasuya, and Yosida) theory, the exchange interaction results from an indirect coupling of the spins through the conduction electrons. An explicit, but rather complicated, expression for the exchange

integral has been derived[1] within the framework of this theory. This expression, which is correct to second order in the interaction between the localized spins and the conduction electrons, depends on the details of the electronic band structure and on certain matrix elements which must be calculated using Bloch functions.

During the past few years, numerical techniques have advanced to the stage where realistic calculations of the exchange integral can be performed and compared with experimental results. These "first-principles" calculations can not only provide a direct means of verifying the theory but could ultimately lead to a better understanding of the connection between the exotic magnetic behavior observed in members of the heavy rare earth series and the details of their energy band structure.

Two such calculations have been carried out thus far, one on gadolinium[2] and the other on erbium.[3] The erbium calculation correctly predicted the spiral spin configuration as well as the turn angle but no direct comparison of the exchange integral was possible because the experimental information is not yet available. The gadolinium calculation correctly predicted the ferromagnetic spin ordering, and the wave-vector dependence of the exchange integral was found to correlate reasonably well with experiment. The disturbing feature of this calculation is that the difference between the values of $J(q)$ at the zone center and zone boundary (the bandwidth) is about a factor of 4 larger than that observed.

To understand the source of this discrepancy, a re-derivation of the exchange integral, which goes beyond second-order perturbation theory, has been carried out for a spin system with n atoms per unit cell. The results of the calculation indicate two possible sources for the discrepancy, as well as a line-broadening effect for spin waves due to the electron-electron interaction.

The major source of the numerical discrepancy between theory and experiment in gadolinium is most probably due to the incorrect use of the double zone scheme to evaluate $J(q)$. Our expression for $J(q)$ for the heavy rare earth series (hcp lattice with two atoms/cell) involves an integration over the first Brillouin zone with due account taken of phase factors that involve the separation of atoms in the unit cell. This expression is not equivalent to the double-zone representation used in the gadolinium calculation. This, of course, could have a major effect on both the q-dependence and the absolute scale of $J(q)$.

Compared to the conventional result, our result for $J(q)$ also contains correction terms which include the effect of electron-electron interactions. These terms have two effects. First, they alter the q-dependence of $J(q)$. Preliminary calculations carried out in collaboration with P.-A. Lindgård of Research Establishment Risø (Denmark) indicate that these correction terms are important only at low q and tend to reduce the discrepancy between theory and experiment. Second, these terms introduce a width to the spin-wave peaks. The source of this width is the same as that which is responsible for the disappearance of spin waves in itinerant electron magnets, namely interaction with Stoner excitations. This effect will not be as important in rare earths as it is in itinerant magnets, but it could produce detectable widths in the spin-wave peaks, especially near the zone boundary.

It appears, therefore, that additional numerical work is needed to establish whether or not the RKKY theory does indeed provide a good "first-principles" theory for magnetism in the heavy rare earth series.

---

1. T. Kasuya, p. 355 in *Magnetism*, vol. 2a, ed. by G. T. Rado and H. H. Suhl, Academic Press, New York, 1950.
2. P.-A. Lindgård, B. N. Harmon, and A. J. Freeman, *Phys. Rev. Lett.* 35, 383 (1975).
3. J. F. Cooke and H. L. Davis, p. 793 in *Proceedings of the Conference on Neutron Scattering*, vol. II, ed. by R. M. Moon, ERDA CONF-760601-P2, Oak Ridge, Tenn., 1976.

CANONICAL TRANSFORM METHOD FOR TREATING STRONGLY ANISOTROPIC MAGNETS

J. F. Cooke P.-A. Lindgård[1]

The theory of magnetism in anisotropic magnets has for many years been based on techniques developed and successfully used for treating isotropic spin systems. For example, conventional spin-wave theory has been applied to anisotropic magnets to obtain a general expression for the spin-wave energy, and this expression has been fitted to experimentally determined dispersion curves, thereby yielding information about exchange integrals and crystal field parameters. The heavy rare earth metals and several magnetic insulators (for example, $CsNiF_3$) are known to have crystal fields and exchange interactions of similar magnitude. It was found that good fits could be found to the zero-field dispersion curves for all of the heavy rare earth series,[2] except for erbium.

Erbium is a special case in that its magnetic structure has a conical arrangement of moments at low temperatures. It was thought that a giant two-ion anisotropy had to be introduced in order to fit the experimental results for erbium.[3] Subsequently, field-dependent measurements[4] on ferromagnetic terbium indicated that a giant two-ion anisotropy probably had to be introduced in many other rare earth metals as well.

The existence of such a large two-ion anisotropy is difficult to understand. It has been known for many years that this type of anisotropy can result from an aspherical charge cloud (nonzero orbital angular momentum) of the electrons which produce the local moment. Rather crude estimates of this effect for the heavy rare earth metals indicated it to be quite small. Other sources of two-ion anisotropy, such as spin-wave-phonon coupling are also expected to be small compared to the isotropic exchange interaction.

In a recent paper, Lindgård[5] suggested that conventional spin-wave theory leads to an inadequate treatment of the single-ion anisotropy and therefore to an incorrect expression for the spin-wave energy, E_q. A systematic perturbation theory based on an expansion in terms of the ratio of the single-ion anisotropy, V_c, to the exchange interaction energy, H_{ex}, was found to yield a new expression for E_q. On the basis of this expression, it was shown that the spin-wave data in erbium and terbium could be explained solely in terms of an isotropic interaction without the introduction of two-ion anisotropy. These results and conclusions were, however, based on an expansion of relevant quantities to first order in V_c/H_{ex}, and it was not clear what effect this limitation had on the analysis. Since V_c/H_{ex} is not in general small, as for example in the rare earth metals, it is important to carry the theory to higher order.

To accomplish this, we have developed a new infinite-order perturbation approach for treating strongly anisotropic magnets. This formalism is based on a canonical transformation of the system into a system with *effective* two-ion anisotropy which, for example, can be treated by conventional spin-wave techniques. In this respect the new formalism is similar to pseudo-spin theories but is simpler to apply because it does not require a complete knowledge of the crystal field and it is not necessary to diagonalize the single-site part of the Hamiltonian completely. The theory is valid for any spin magnitude and for arbitrary crystal fields and in principle can be carried to any order of perturbation in the expansion parameter V_c/H_{ex}.

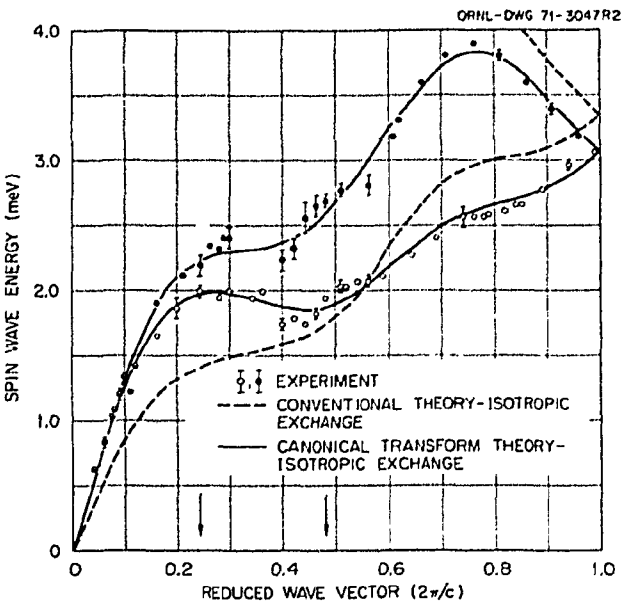

Fig. 1.20. Spin-wave energies for erbium metal.

An expression for the spin-wave energy for the general conical magnetic moment configuration with arbitrary crystal field has been derived using this formalism. It was found that an analysis of the transverse spin-wave spectra can at most result in a determination of a renormalized exchange integral and two renormalized anisotropy constants. These parameters are not simply related to the fundamental parameters (exchange and crystal field) which appear in the original Hamiltonian. Explicit expressions for these parameters have been determined to second order in the ratio of crystal field to exchange field.

A comparison of spin-wave energies in erbium obtained from the canonical transformation (solid curve) and conventional spin-wave (dashed curve) theories is given in Fig. 1.20. Both results were obtained from a Hamiltonian with *isotropic* exchange (and general crystal field) and represent the best fit, in a least squares sense, to the experimental points of Nicklow et al.[3] The agreement between the canonical transform result and the experimental data clearly eliminates the necessity of having to introduce a giant two-ion anisotropic exchange. We have also found that the magnetic field dependence of the spin-wave energy agrees qualitatively with the observations on terbium.

We conclude that a substantial part of the large two-ion anisotropy, which had been introduced to describe the spin-wave spectra in the heavy rare earth

series, actually resulted from the analysis of the spin-wave data in terms of an incorrect expression for the spin-wave energy and not from any physical source.

---

1. Research Establishment Risø, Roskilde, Denmark.
2. A. R. Mackintosh and H. B. Moller, *Adv. Phys.* 25, 187 (1976).
3. R. M. Nicklow et al., *Phys. Rev. Lett.* 27, 334 (1971).
4. J. Jensen, J. G. Houmann, and H. B. Moller, *Phys. Rev. B* 12, 303 (1975).
5. P.-A. Lindgård, *Phys. Rev. Lett.* 36, 385 (1976).

LATTICE DYNAMICS

FIRST-PRINCIPLES PHONON CALCULATIONS IN TRANSITION METALS

J. F. Cooke H. L. Davis Mark Mostoller

The interrelationship of superconductivity and phonon anomalies in bcc transition metal systems with high transition temperatures has been a topic of considerable interest during the past few years. A number of phenomenological models have been proposed for describing these anomalies, but they do not provide direct information about the fundamental relationship between the anomalies and superconductivity.

One method of attacking this problem is to make use of the dielectric response formalism. This is a "first-principles" approach which relates the dynamical matrix to the inverse of the dielectric screening matrix, thereby providing a direct link between the phonon frequencies and the electronic properties of the system. In its most conventional form, this theory presents some rather formidable convergence problems, and a number of attempts have been made to reformulate the theory in order to avoid them. These approaches have met with varying degrees of success but, as yet, no complete, first-principles calculation of the phonon spectra has been carried out.

Our approach to this problem is to use the conventional formulation of the problem combined with an exact expression for the matrix elements which appear in the theory to obtain an analytic (and closed-form) expression for the dynamical matrix. This exact result is made possible by making use of the explicit form of the electronic wave functions generated by the Korringa-Kohn-Rostocker (KKR) band structure formalism. This not only enables us to analytically invert the dielectric screening matrix but also to avoid approximations associated with multicenter integrals.

The major difficulty with this approach is that it leads to reciprocal lattice sums which converge rather slowly. Fortunately, these sums can be transformed to sums over the direct lattice, which converge much faster. Preliminary numerical calculations indicate that contributions from *s*- and *p*-symmetry terms outside the muffin tin cannot be ignored. Incorporation of terms of this type into the calculation is straightforward but would require a prohibitive amount of computer time, and therefore, a number of approximations are being investigated.

As the result of our investigations thus far, it appears that realistic first-principles calculations of phonon spectra in transition metal systems are within our grasp, thereby providing a powerful tool for studying lattice vibrations and superconductivity in transition metal systems.

ELEMENTARY EXCITATIONS IN LARGE MOLECULES

Mark Mostoller Theodore Kaplan
R. C. Ward[1]

As described in two other contributions to this report,[2] recursion procedures based upon the Lanczos algorithm can be used to calculate certain electronic and vibrational properties of bulk and surface atoms. For the electronic or vibrational spectra of atoms in large molecules, we have been investigating an iterative variation of the Lanczos method proposed by Paige and Saunders.[3] We have been testing the method by applying it to the vibrational modes of hypothetical large molecules, namely cubic alloy clusters of tens to hundreds of atoms. We plan to apply the iterative Lanczos procedure to elementary excitations in real rather than hypothetical molecules after thorough testing on the model systems.

As outlined in ref. 2, the Lanczos algorithm defines an orthonormal set of basis vectors which tridiagonalizes the Hamiltonian matrix H (or the dynamical matrix D for vibrational problems). In contrast to conventional methods of matrix inversion, the Lanczos procedure has two major computational advantages. First, the whole matrix H need not be stored. Instead, space must be provided only for three vectors and two linear arrays of tridiagonal matrix elements. Storage requirements thus increase linearly rather than quadratically with the

rank n of the matrix. Second, with suitable programming, the number of operations performed increases as the square of the rank of the matrix, rather than as the cube.

The Lanczos procedure as we have been using it also has two major limitations. First, each application yields only one particular element of the inverse, restricting it to such applications as density-of-states calculations or calculations of selected correlation functions. Second, although in principle the Lanczos procedure generates an orthonormal set of vectors, in practice orthogonality begins to be lost after something of the order of 30 to 100 vectors have been generated by the computer. This latter disadvantage is a computational artifact that would not occur on a computer which had infinite precision.

The iterative Lanczos approach deals with the nonorthogonality of the vectors generated by the computer by expressing the desired element of the inverse matrix as an approximate solution plus a residual. If the residual is larger than a prescribed minimum, another vector is generated, and this cycle is repeated until convergence is obtained. The procedure may in fact generate more vectors than the rank of the matrix involved.

We have compared the results of straight and iterative Lanczos calculations with those of conventional matrix inversion techniques for vibrational modes in cubic alloy clusters of up to 65 atoms (and hence 195 modes). Significant errors are found in the straight Lanczos results, but the iterative Lanczos calculations converge to the "exact" results with an accuracy corresponding to the prescribed residual. Furthermore, the iterative Lanczos procedure is significantly faster than the conventional techniques for the larger matrices investigated. Figure 1.21 shows the xx vibrational density of states for the central atom in a 321 atom fcc alloy "molecule" as calculated by the iterative Lanczos procedure. The calculation, which was done in REAL*8 arithmetic on an IBM 360-91 computer, required less than 0.8 megabytes of core and less than 5 min of computer time. No corresponding result obtained by conventional techniques is shown, since it would require roughly 4 megabytes of core just to store the upper right half of the 963 × 963 dynamical matrix for this cluster, that is, about twice the core available.

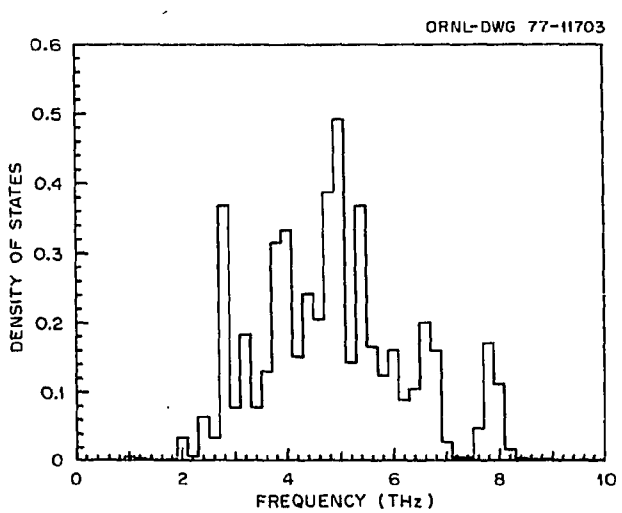

Fig. 1.21. Vibrational density of states of the central atom in an fcc alloy "molecule" of 321 atoms; the cluster had a free surface. First-nearest-neighbor forces corresponding to a $Cu_{1-c}Al_c$ alloy were used, the concentration was $c = 0.087$, and a copper atom was at the central site.

1. Computer Sciences Division, UCC-ND.

2. Mark Mostoller and Theodore Kaplan, "Cluster Calculations: Simulation of Bulk Properties"; Mark Mostoller and Theodore Kaplan, "Lattice Vibrations at Surfaces," this report.

3. C. C. Paige and M. A. Saunders, *SIAM J. Numer. Anal.* 12, 617 (1975).

PHONON–INTERNAL MODE HYBRIDIZATION IN KCl:CN^-

R. F. Wood Mark Mostoller

Recent theoretical[1,2] and experimental[3-5] work has shown that the resonant mixing of defect internal modes with lattice phonons can produce striking effects in the one-phonon coherent neutron scattering cross section at very low defect concentrations. The first such system studied by neutron scattering was KCl doped with substitutional CN^- ion impurities. For KCl:CN^-, Walton, Mook, and Nicklow[3] reported multipeaked structure at 5 K for the acoustic modes of E_g character propagating along the $\langle 110 \rangle$ direction and polarized in the $\langle 1\bar{1}0 \rangle$ direction; this structure was not present at room temperature. Nicklow[5] has since undertaken a more comprehensive study of the KCl:CN^- system, and he finds a two-peaked structure for this branch at low temperatures. The intensity shifts from the lower frequency peak to the higher frequency peak as the wave vector is varied through resonance, which occurs at approximately $q = (2\pi/a)$ (0.08, 0.08, 0), $\nu = 0.5$ THz. Again, the resonance structure disappears as the temperature is increased, although some shifts in frequency are still observed at 120 K.

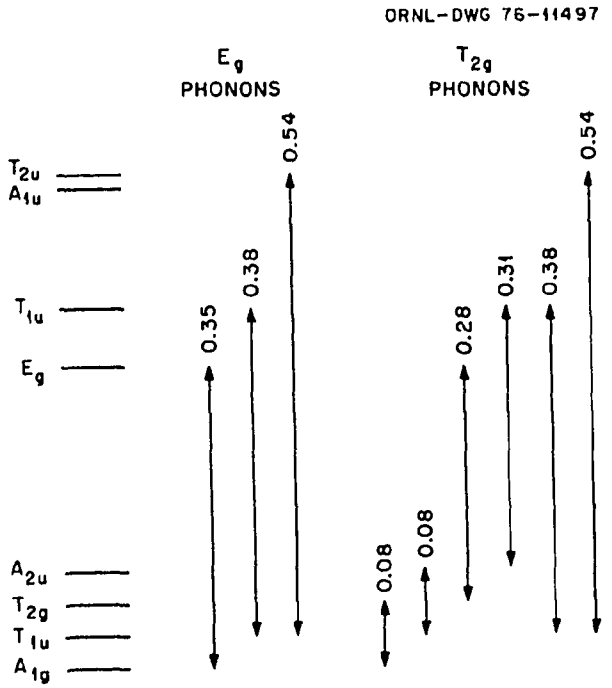

Fig. 1.22. Approximate level spacings and allowed E_g, T_{2g} transitions in terahertz for CN^- in KCl, from Beyeler (ref. 6).

Figure 1.22 shows an approximate energy level diagram for an isolated CN^- ion in KCl, taken from the work of Beyeler.[6] The impurity behaves like a hindered rotator, whose ground state is a tunnel-split multiplet involving the eight equivalent ⟨111⟩ orientations. Also shown in the figure are the allowed transitions among the low-lying impurity states which involve E_g and T_{2g} phonons; ultrasonic measurements by Byer and Sack[7] indicate particularly strong coupling to these lattice modes. The observed E_g resonance frequency of $\nu \approx 0.5$ THz is consistent with one of the allowed transitions shown in Fig. 1.22.

Klein[8] has treated the resonant scattering of lattice modes by a substitutional impurity that has two energy levels at $\pm h\nu_0/2$ in the static lattice. For our purposes, the effects of such an impurity interacting with lattice modes of the host crystal can be summarized as follows. First, the neutron scattering cross section can exhibit a two-peaked structure or a resonance frequency shift and line broadening, depending on the size of the damping of the interlevel transition frequency in the vibrating crystal. Second, the elastic constant for sound waves of the appropriate polarization is reduced by the resonant lattice-impurity coupling. Third, both of the aforementioned effects are strongly temperature dependent, decreasing in magnitude as the temperature increases and the population difference between the two levels decreases.

As indicated in Fig. 1.22, the CN^- ion in KCl is a multilevel impurity. A theory for the multilevel impurity can be developed along the lines used by Klein for the two-level impurity, and there are two major new qualitative features of this more complicated treatment. First, a lattice mode of a given local symmetry may have a resonant coupling to two or more interlevel transitions, and second, there are temperature-independent as well as temperature-dependent self-energy terms. A multilevel impurity can therefore produce more complicated structure and temperature dependence in the neutron scattering cross section than a two-level impurity.

We have used the two-level model for the KCl:CN^- system, with coupling between the impurity transition and the E_g modes of the six first nearest neighbors of the CN^- ions. The coupling constant and the bare transition frequency ν_0 were treated as adjustable parameters. Calculated and experimental results for the neutron scattering cross section for phonons propagating along the ⟨110⟩ direction and polarized in the ⟨1$\bar{1}$0⟩ direction are shown in Fig. 1.23. The agreement between calculated and ex-

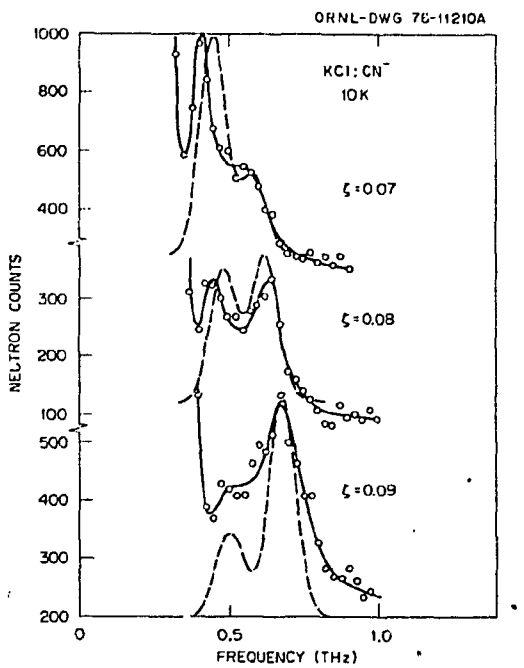

Fig. 1.23. Neutron scattering from KCl containing 3700 ppm CN^- ion impurities. The results shown are for phonons with wave vectors $\mathbf{q} = (2\pi/a)(\zeta,\zeta,0)$, polarized in the [1$\bar{1}$0] direction. The circles are experimental data points to which the solid curves have been fit visually; the dashed curves give the theoretical results. The sharp increase in neutron counts at low frequencies is due to Bragg-peak contamination.

perimental results is reasonably good, although the calculated peak splittings are somewhat too small. The calculated and observed temperature dependences of the neutron scattering cross section are also in reasonably good overall agreement. However, there seems to be some evidence that the two-level model underestimates the magnitude of the residual shifts in the phonon dispersion curves which are still observed at 120 K.

We also calculated the fractional change in the elastic constant of interest, which is $c_{11} - c_{12}$, as a function of temperature. The overall shape of the curve was similar to that observed experimentally,[7] but the values of the elastic constant changes, like the peak splittings, were somewhat too small.

We conclude that the simple two-level impurity model gives reasonably good agreement with most of the experimental data available at present for the E_g modes of KCl:CN^-. More extensive experimental results that unambiguously test the predictions of the two-level model would be very useful.

1. R. F. Wood and Mark Mostoller, *Phys. Rev. Lett.* 35, 45 (1975).
2. H. R. Schober, V. K. Tewary, and P. H. Dederichs, *Z. Phys. B* 21, 255 (1975).
3. D. Walton, H. A. Mook, and R. M. Nicklow, *Phys. Rev. Lett.* 33, 412 (1974).
4. R. M. Nicklow et al., *Phys. Rev. Lett.* 35, 1444 (1975).
5. R. M. Nicklow, p. 117 in *Proceedings of the Conference on Neutron Scattering*, vol. I, ed. by R. M. Moon, ERDA CONF-760601-P1, Oak Ridge, Tenn., 1976.
6. H. U. Beyeler, *Phys. Status Solidi* 52, 419 (1972); *Phys. Rev. B* 11, 3078 (1975).
7. N. E. Byer and H. E. Sack, *Phys. Status Solidi* 30, 569 (1968).
8. M. V. Klein, *Phys. Rev.* 186, 839 (1969).

FIRST-ORDER, INDUCED RAMAN SCATTERING FROM IMPURITIES

R. F. Wood Mark Mostoller

First-order Raman scattering is normally forbidden by symmetry in crystals with the NaCl structure. However, introduction of a substitutional impurity into the lattice destroys the translational symmetry, and Raman scattering from vibrational motion of the neighbors of the impurity ion can be observed.

Calculations of the first-order, induced Raman scattering are based on localized-perturbation theory which assumes that the addition of an impurity atom to or the removal of an ion from the host lattice significantly affects only a relatively small region of the lattice around the defect site. The equations of motion of a crystal containing a single substitutional impurity or vacancy in an otherwise perfect lattice are given in matrix form by

$$[(M_0 + \delta M)\omega^2 - (K_0 + \delta K)]\mathbf{u} = 0 , \qquad (1)$$

where M_0 and K_0 are, respectively, the mass and force constant matrices of the unperturbed lattice, δM and δK are matrices of the mass and force constant changes due to the presence of the defect, and $\mathbf{u}$ is the vector of Cartesian displacements of the ions. Equation 1 can be cast in a different form,

$$(1 + G^0\Delta)\mathbf{u} = 0 , \qquad (2)$$

where $G^0 = (M_0\omega^2 - K_0)^{-1}$ is the Green's function matrix for the perfect crystal, and $\Delta = \delta M\omega^2 - \delta K$ is often referred to as the defect matrix. The Green's function matrix of the perturbed crystal can then be expressed in terms of G^0 and Δ by

$$G = [M_0\omega^2 - K_0 + \Delta]^{-1} = (1 + G^0\Delta)^{-1}G^0 . \qquad (3)$$

Since an impurity destroys the translational symmetry of the lattice, the spatially periodic phonons of the perfect crystal are no longer eigenfunctions of the problem. It is therefore natural to fall back on the point symmetry properties of the defect and to introduce combinations of ionic displacements that are adapted to that symmetry. These orthonormalized, linear combinations of Cartesian displacements will be referred to as symmetry coordinates and written as

$$Q_n(\Gamma p) = \sum_{l\alpha} c(n\Gamma p;\, l\alpha)u_\alpha(l) , \qquad (4)$$

where Γ gives the irreducible representation according to which the symmetry coordinate transforms, n is an index that refers to shells of equivalent ions in the crystal, p labels the orthogonal components that can be constructed for each n and Γ, l is a site, and α is a Cartesian index. The notation is not complete because the allowed motions of some shells may contain more than one occurrence of some of the irreducible representations; for simplicity this possibility will be ignored here.

An element of the Green's function matrix of the perfect crystal can be expressed in the symmetry coordinate representation. We use the notation

$$G_{nm}{}^0(\omega^2, \Gamma p) \equiv (Q_n(\Gamma p)|\, G^0|\, Q_m(\Gamma p) \qquad (5)$$

and note that the Green's function matrix, like the dynamical matrix, is diagonal in Γ and p. Of course,

G^0 is also diagonal in the Bloch function representation of the unperturbed phonons, and it is convenient to utilize this property whenever possible.

The intensity of the Raman scattering is proportional to quantities of the form

$$I_{\alpha\gamma,\beta\lambda} = \sum_{\Gamma p n m} \frac{\partial P_{\alpha\gamma}}{\partial Q_n(\Gamma p)} \frac{\partial P_{\beta\lambda}}{\partial Q_m(\Gamma p)} \rho_{nm}(\omega, \Gamma)/2\omega \ . \quad (6)$$

$P_{\alpha\gamma}$ is a cartesian component of the polarizability tensor. The quantity $\rho_{nn}(\omega, \Gamma)$ is the perturbed, normalized projected density of states for shell n, and for $n \neq m$, $\rho_{nm}(\omega, \Gamma)$ is a cross term describing intershell coupling:

$$\rho_{nm}(\omega, \Gamma) = \frac{2\omega}{\pi} \lim_{\epsilon \to 0^+} \mathrm{Im} \langle Q_n(\Gamma p) | \, G(\omega^2 + i\epsilon) | \, Q_m(\Gamma p) \rangle$$

$$\equiv \frac{2\omega}{\pi} \mathrm{Im} \ G_{nm}(\omega^2, \Gamma) \ . \quad (7)$$

The indices α, γ, β, and λ in Eq. (6) each run over x, y, z, giving 81 of the $I_{\alpha\gamma,\beta\lambda}$ terms, but of these only three terms can be expressed as linear combinations of the A_{1g}, E_g, and T_{2g} projected densities of states. Furthermore, by appropriate choices of geometry for the Raman experiments, it is possible to extract the A_{1g}, E_g, and T_{2g} densities individually. Thus the defect-induced, first-order Raman scattering is a direct measure of the perturbed density of states for those coordinates Q that have nonzero polarizability derivatives. The perturbed density of states will exhibit peaks at the frequencies of localized or resonance modes, if any, and may also manifest the critical points or Van Hove singularities associated with pure-crystal phonon spectra.

As shown by Eq. (3), in order to calculate the matrix elements of G, it is necessary to determine G^0 and Δ. The calculation of the matrix elements of G^0 requires knowledge of the eigenfrequencies and eigenvectors of the perfect crystal. These can be obtained from some model for the lattice dynamics of the perfect crystal, for example, the shell model. The imaginary part of $G^0(\omega^2, \Gamma p)$ can be found from the equation

$$\mathrm{Im} \ G_{nm}{}^0(\omega^2, \Gamma p)$$

$$= \pi \sum_{qj} P_{nm}(\mathbf{q}j; \Gamma p) \delta[\omega^2 - \omega^2(\mathbf{q}j)] \ , \quad (8)$$

with

$$P_{nm}(\mathbf{q}j; \Gamma p) \equiv \langle Q_n(\Gamma p) | \, \mathrm{v}(\mathbf{q}j) \rangle \langle \mathrm{v}(\mathbf{q}j) | \, Q_m(\Gamma p) \rangle \ , \quad (9)$$

where $\mathrm{v}(\mathbf{q}j)$ is the phonon eigenvector of the perfect crystal with wavevector q and branch index j. The real part of $G^0(\omega^2, \Gamma p)$ can be found from the imaginary part by a Kramers-Kronig transform. The elements of the defect matrix can be estimated from a suitable potential model, or they may be treated as adjustable parameters.

Computer programs[1] implementing the above theory have been constructed and refined over a period of years, and during the past year they have been further developed and used for the following three problems:

Ni^{2+} ions and Li^+ Vacancies in LiCl (ref. 2)

In work reported last year, Bates and Shankle[3] measured the impurity-induced, first-order Raman spectra of LiCl containing substitutional Ni^{2+} impurities. To maintain overall charge neutrality, compensating Li^+ vacancies must be present in these crystals. Comparison of quenched and annealed samples of LiCl:Ni^{2+}, of crystals with different Ni^{2+} concentrations, and of the observed Raman spectra with group theoretical predictions indicated that the Ni^{2+} ions and compensating cation vacancies are present as isolated defects rather than as impurity-vacancy complexes. At 12 K, first-order Raman bands were observed at 247, 216, 161, and 122 cm^{-1} and assigned to A_{1g}, T_{2g}, E_g, and T_{2g} phonon modes respectively. Since the allowed modes of the nearest neighbor of a substitutional Ni^{2+} impurity include one A_{1g}, E_g, and T_{2g} representation, one of the observed T_{2g} bands was provisionally associated with the Li^+ vacancies.

We have studied the Raman scattering induced by Ni^{2+} ions and cation vacancies in LiCl theoretically, using a classical ionic crystal model[4] to estimate local force constant changes for the various symmetry modes around the two defects. Because no satisfactory Born-Mayer parameters for the Ni^{2+}-Cl^- interaction were available and because the Ni^{2+} ion may give rise to relatively long-range perturbations, we do not regard these results as more than a semiquantitative guide. Furthermore, the only shell model parameters available for LiCl are those obtained by Haridasan[5] from fitting optical and

elastic constant data. Our calculations strongly suggest that the observed Raman bands at 247 and 216 cm^{-1} are due to A_{1g} and T_{2g} modes, respectively, of the neighbors of Ni^{2+} impurities, while the band at 161 cm^{-1} is an E_g peak produced by neighbors of Li^+ vacancies. However, no T_{2g} mode around cation vacancies could be found within the framework of the model which gave rise to a single sharp band at 122 cm^{-1}. We are therefore unable to show conclusively that our assignment of the other observed bands is correct, although the evidence for it from the A_{1g} and E_g modes seems rather strong.

Carbon Vacancies in TiC

Klein[6] and collaborators at the University of Illinois have recently measured the first-order, induced Raman scattering from vacancies in TiC and provided us with their results. Because these results have not yet been submitted for publication, we are unable to give here a detailed comparison between theory and experiment. However, we can briefly describe the calculations and their results.

The eigenvectors and eigenfrequencies for the phonons of the perfect crystal were generated using the parameters of a screened-shell model fitted to the data of Gompf et al.[7] Symmetry coordinates for A_{1g}, E_g, and T_{2g} modes were constructed from the Cartesian displacements of the ions in the first, second, and fourth shells of neighbors of the carbon vacancies. The symmetrized force constant changes were treated as adjustable parameters. To attain agreement with a number of features of the experimental data, it was necessary to include the polarizability derivatives of the second and fourth neighbors. The calculations suggest that the experimentally observed spectra are always mixtures of A_{1g}, E_g, and T_{2g} components, regardless of the geometry used. This could come about because of the density of carbon vacancies (>2%) in the samples.

F Centers in CaO

The measured induced Raman scattering spectra from *F* centers in CaO and calculations to fit them are reported elsewhere[8] in this annual report.

1. A more complete discussion of the computational details can be found in R. F. Wood, p. 119 in *Methods in Computational Physics*, vol. 15, ed. by B. Alder, S. Fernbach, and M. Rotenberg, Academic Press, New York, 1976.
2. J. B. Bates et al., *Phys. Rev. B* 15, 3267 (1977).
3. J. B. Bates and G. E. Shankle, *Solid State Div. Annu. Prog. Rep. Dec. 31, 1975*, ORNL-5135, p. 55.
4. Mark Mostoller and R. F. Wood, *Phys. Rev. B* 7, 3935 (1973).
5. T. M. Haridasan, *Opt. Commun.* 9, 296 (1973).
6. M.V. Klein, private communication.
7. F. Gompf, et al., p. 129 in *Proceedings of the Conference on Neutron Scattering*, vol. I, ed. by R. M. Moon, ERDA CONF-760601-P1, Oak Ridge, Tenn., 1976.
8. J. B. Bates and R. F. Wood, "Raman Scattering from *F* Centers in CaO," this report.

ON THE COMPUTATION OF FEYNMAN PATH INTEGRALS

Theodore Kaplan L. J. Gray[1]

Since Feynman's introduction of the path integral derivation of quantum mechanics in 1948,[2] the path integral has been used as a theoretical tool throughout the various fields of physics.[3] However, for computational purposes, the path integral has remained exceedingly difficult to handle. Most previous computational methods have relied on evaluating multidimensional integrals of large dimension.[4,5] Using an approach which is quite similar to the Augmented Space Formalism[6,7] in the theory of disordered systems, we have expressed the path integral as the matrix element of an operator and thus have replaced the difficult numerical integration by a problem in linear algebra.

We have completed calculations using our method for the Green's function of a one-dimensional harmonic oscillator—a problem whose exact solution is known. Our computed solutions are in excellent agreement with the exact solution. Work is now in progress on the anharmonic oscillator.

1. Computer Sciences Division, UCC-ND.
2. R. P. Feynman, *Rev. Mod. Phys.* 20, 367–87 (1948).
3. R. P. Feynman and A. R. Hibbs, *Quantum Mechanics and Path Integrals*, McGraw-Hill, New York, 1965.
4. L. D. Fosdick, *J. Math. Phys.* 3, 1251 (1962).
5. L. D. Fosdick and H. F. Jordan, *J. Comput. Phys.* 3, 1–16 (1968).
6. T. Kaplan and L. J. Gray, *Phys. Rev. B* 14, 3462 (1976).
7. T. Kaplan and L. J. Gray, *Phys. Rev. B* 15, 3260 (1977).

A COMMENT ON THE DENSITY OF STATES OF RANDOM ALLOYS

M.V.K. Ülehla[1] Theodore Kaplan

Using the Augmented Space Formalism,[2,3] the problem of calculating the configurationally averaged density of states of a disordered system can

be reduced to evaluating a single matrix element of the inverse of a nonrandom Hermetian matrix. We have employed the "self-avoiding-path" technique[4,5] to approximate the desired element of this inverse matrix.

Using this approach, we calculated the density of states of a random substitutional binary alloy in three dimensions with diagonal and off-diagonal disorder. It was found that the "self-avoiding-path" method depends critically on the procedures adopted for terminating the infinite number of self-avoiding paths appearing in the expansion of the inverse matrix element. Only for the simple termination based on a Cayley tree topology can we be certain of producing an analytic result. This type of termination gives adequate results only for the special case of diagonal disorder. A more sophisticated method of termination, which yields analytic results and which is adequate for treating off-diagonal disorder as well, remains the goal of our on-going analysis.

---

1. Eugene P. Wigner Fellow.
2. A. Mookerjee, *J. Phys. C* **6**, L205 (1973); *J. Phys. C* **6**, 1340 (1973).
3. T. Kaplan and L. J. Gray, *Phys. Rev. B* **14**, 3462 (1976); *Phys. Rev. B* **15**, 3260 (1977).
4. A. R. Bishop and A. Mookerjee, *J. Phys. C* **7**, 2165 (1974).
5. P. W. Anderson, *Phys. Rev.* **109**, 1492 (1958).